A comparison and summary of aerosol optical properties as observed in situ from aircraft, ship, and land during ACE-Asia

Sarah J. Doherty,[1,2] Patricia K. Quinn,[3] Anne Jefferson,[4] Christian M. Carrico,[5,6] Theodore L. Anderson,[1] and Dean Hegg[1]

[1] During the ACE-Asia campaign in March–May 2001, in situ measurements of aerosol optical properties were made from multiple airborne and land- or ship-based platforms. Using a suite of direct interplatform comparisons and a campaign-wide statistical comparison, we test the precision of these measurements, and we determine whether the platforms sampled similar aerosol. Data included in the study are from the National Center for Atmospheric Research C-130 aircraft; the CIRPAS Twin Otter aircraft; the National Oceanographic and Atmospheric Administration (NOAA) ship R.V. Ronald H. Brown; and the Gosan surface station on Jeju Island, located off the southern tip of South Korea. Comparisons were made of total and submicron light scattering at 450, 550, and 700 nm; total and submicron absorption at 550 nm; the Ångström exponent; single scatter albedo of the total aerosol, submicron and supermicron aerosol at 550 nm; hemispheric backscatter fraction at 550 nm; and light scattering hygroscopic growth at 550 nm. For the campaign-wide comparison, the data are broken down by light scattering fine mode fraction since the aerosol in the ACE-Asia study region were a variable mix of pollution, dust, and sea salt. Finally, we calculate how the observed uncertainties in the aerosol optical properties propagate to uncertainties in top-of-atmosphere radiative forcing. Single scatter albedo showed excellent agreement among all platforms other than the Twin Otter, with discrepancies generally <0.02. These data sets combine to give campaign-wide values of single scatter albedo of 0.885 ± 0.023 for the submicron aerosol (i.e. pollution) and 0.957 ± 0.031 for the supermicron aerosol (which, for these data, was predominantly dust). The data also indicated that, as expected, the Low Turbulent Inlet on the C-130 produced enhanced concentrations of coarse mode aerosol. There also may have been significant coarse mode particle losses on the other platforms. These effects combined to produce generally lower fine mode fractions and Ångström exponents on the C-130 than on the other platforms. Large discrepancies in hemispheric backscatter fraction and light scattering hygroscopic growth were observed in both the side-by-side and statistical comparisons. We are not able to explain these differences, though possible causes are discussed. Studies of the TSI, Inc. nephelometer backscatter measurement and of the two methods used here to measure hygroscopic growth are needed to clarify the source of these observed discrepancies. A better understanding of the effects of nonsphericity on hemispheric backscatter fraction is also needed.

[1]Department of Atmospheric Science, University of Washington, Seattle, Washington, USA.
[2]Formerly Sarah J. Masonis.
[3]Pacific Marine Environmental Laboratory, NOAA, Seattle, Washington, USA.
[4]Climate Monitoring and Diagnostics Laboratory, NOAA, Boulder, Colorado, USA.
[5]Department of Atmospheric Science, Colorado State University, Fort Collins, Colorado, USA.
[6]Also at Department of Civil and Environmental Engineering, University of Illinois, Urbana, Illinois, USA.

1. Introduction

[2] In March to May 2001, the third in a series of Aerosol Characterization Experiments (ACE) took place in the Asian region [*Huebert et al.*, 2003]. The ACE studies are an activity of the International Global Atmospheric Chemistry (IGAC) Project operating under the auspices of the International Geosphere Biosphere Program (IGBP) and the Commission on Atmospheric Chemistry and Global Pollution (CACGP). During ACE-Asia, in situ measurements of aerosol optical properties were made from multiple research platforms in the eastern Asian region. A focus of these

measurements was to constrain the optical properties of aerosols, particularly pollutants and desert dust, in the region around eastern China, Korea, and Japan so that they can be more accurately represented in radiative forcing models. Each of the platforms involved in ACE-Asia covered a different geographic area and, in some cases, different vertical segments of the atmosphere. The most comprehensive set of information about the aerosol in this region can therefore be gained by viewing them as a collective set. First, however, we need to test whether these platforms made equivalent measurements of the aerosol.

[3] We do this here by comparing in situ optical measurements from airborne and surface platforms using two approaches: a) we compare measurements from times where the two platforms were nearly colocated ("direct interplatform comparisons"), and b) we compare campaign-wide data sets ("ensemble comparison"). Ideally, the colocated comparisons tell us if there is a bias or error in the measurements on one or more of the platforms. If the direct interplatform comparisons agree well, the ensemble comparison should tell us to what degree the different platforms were sampling similar aerosol, allowing us to ascertain how to best combine the disparate data sets for a better large-scale picture of the aerosol in the study region. If multiple platforms' measurements give similar results for the optical properties of the aerosol then we can feel more confident that these data are both accurate and regionally representative. Closure tests – wherein different methods are used to derive a common parameter – are also vital to assessing our ability to characterize aerosol properties. Others have tested for closure between the ACE-Asia data sets from a given platform. The results of these studies are considered here to the degree that they help us interpret the results of our comparisons of in situ measurements.

[4] While there were many field stations involved in the ACE-Asia campaign, the four included in this analysis were selected because of the uniformity and comprehensiveness of their measurements. They are: the National Center for Atmospheric Research (NCAR) C-130 aircraft; the CIRPAS Twin Otter aircraft; the National Oceanographic and Atmospheric Administration (NOAA) ship R.V. Ronald H. Brown; and the Gosan surface station on Jeju Island, located off the southern tip of South Korea. In situ optical measurements were made on these platforms by researchers from the University of Washington and University of Hawaii [C-130]; the University of Washington [Twin Otter]; the NOAA Pacific Marine Environmental Lab (PMEL) and the University of Illinois [Ron Brown]; and the NOAA Climate Monitoring and Diagnostics Lab (CMDL) [Gosan].

[5] The analysis herein is analogous to the comparison study by *Clarke et al.* [2002] of aerosol properties as measured in situ during the Indian Ocean Experiment (INDOEX), and it should be viewed as complementary to their work. For the INDOEX analysis comparisons were also made between aircraft, ship and surface stations. Two of the groups that made in situ optical measurements during INDOEX also participated in the ACE-Asia project (i.e. NOAA-PMEL, also on the Ron Brown; and NOAA-CMDL). Repeated comparisons from successive campaigns such as INDOEX and ACE-Asia allow us to a) apply lessons learned in the earlier analysis to later campaigns

and b) assess the accuracy of commonly used measurement techniques under different sampling scenarios and for a range of aerosol types. For example, during INDOEX the aerosol was dominated by fine mode pollution whereas for ACE-Asia the samples were a mix of fine mode aerosol (primarily pollution) and coarse mode aerosol (primarily dust, but sometimes sea salt). The presence of a significant coarse mode complicates the in situ measurements because of the difficulties in efficiently passing large aerosol through inlets and plumbing, so the comparisons for ACE-Asia are a more rigorous test of these measurements than were the INDOEX comparisons.

2. Direct Interplatform Comparison Coordination

[6] The goals and strategy of the ACE-Asia campaign are described in detail by *Huebert et al.* [2003]. Part of the campaign included an effort to colocate platforms whenever possible, keeping in mind that there were many scientific goals driving the aircraft and ship navigational planning, specifically for the purpose of comparing and integrating measurements on different platforms. In some cases there were restrictions on where the aircraft and ship could go so that, for example, the Ron Brown was never allowed to pass very close to Jeju Island. The resulting set of interplatform comparison times and locations is shown in Table 1.

[7] For all surface station fly-bys the C-130 and Twin Otter aircraft flew over the ocean surface at an altitude of $\sim$35–55 m above sea level (ASL) (Table 1). The Ron Brown stack inlet is 18 m ASL, so the aircraft samples were always from $\sim$15–35 m higher up in the atmosphere than were the ship samples. The Gosan station is at the top of a 72 m cliff, and the stack inlet for the optical instruments was 10 m above the ground. This 82 m is actually higher than the C-130 inlet altitude during fly-bys. However, air on the ocean surface will be lifted as it passes over the island so that the altitude the sampled air was at when it was over the ocean is ambiguous. Especially when winds were strong, flow over the island probably was not laminar. In the case of a strong westerly wind the air sampled at Gosan likely was turbulent and may have contained dirt, dust or other material from the up-slope below the station. It is also known that diesel buses and trucks would occasionally come through the area, although no official record was kept of when local contamination might be a problem.

[8] Below we outline the times when there were opportunities for direct interplatform comparisons. For three of these periods, optical data from one of the platforms are not available (C-130/Gosan on 24 April: Gosan data not available; C-130/Twin Otter on 04 April: Twin Otter data not available; Twin Otter/Ron Brown on 08 April: Twin Otter data not available). We include their description here anyway for completeness, as there are other parameters (i.e. chemical and microphysical) that could be compared in later studies using these interplatform comparison times.

2.1. Selection of Time Periods Used in Aircraft Fly-Bys of Surface Stations

[9] For the aircraft/surface station comparisons, we restricted ourselves to using data when the two platforms were within 35 km horizontally. This provided us with

Table 1. Dates, Research Flight Numbers (C-130 and Twin Otter), Sample Periods, Platform Separation Distance, Wind Data, and Sampling Altitude Are Shown for Direct Interplatform Comparisons[a]

Platf. #1, Platf. #2	Date	RF#	Time, UTC Platform #1	Time, UTC Platform #2	Dist., km	Wind, m/s	Wind Direction	Inlet Altitude, m
C-130, Gosan	6 April	04	02:06:34–02:15:26	01:10:54–03:50:19	2.7	6.9, 5.8	75, 147[b]	52, 82[c]
	12 April	07	01:40:40–01:49:58	00:45:38–03:24:35	1.9	11.5, 15.4	298, 320	39, 82[c]
	12 April	07	07:03:00–07:11:00	06:23:05–08:45:46	1.7	10.4, 11.6	276, 307	44, 82[c]
	18 April	10	04:51:14–05:00:12	03:55:52–06:25:13	4.4	3.9, 5.2	298, 333	52, 82[c]
	18 April	10	05:12:50–05:21:60	03:58:43–07:10:29	4.9	4.4, 5.2	308, 333	51, 82[c]
	24 April	13	06:54:40–07:04:46	05:06:22–08:09:50	2.8	9.4, 10.0	343, 14	36, 82[c]
	2 May	18	02:47:58–02:56:24	02:04:56–04:31:18	2.9	4.6, 6.0	359, 15	46, 82[c]
C-130, R. Brown	4 April	03	05:45:06–05:52:14	04:16:01–06:24:52	1.1	7.8, 6.9	40, 31	45, 15
	8 April	05	04:25:18–04:31:08	02:05:13–04:41:33	0.3	4.7, 4.4	123, 118	39, 15
	13 April	08	01:53:26–02:01:46	00:53:45–02:42:51	4.4	10.5, 9.1	268, 266	49, 15
	17 April	09	07:08:14–07:14:00	03:39:36–07:08:14	3.0	2.9, 2.8	77, 83	48, 15
	17 April	09	07:32:26–07:40:46	04:41:41–09:18:27	8.1	2.7, 3.2	69, 92	48, 15
T. O., R. Brown	6 April	04	03:19:22–03:33:44	01:48:01–03:47:57	0.3	4.0, 5.2	n/a, 63	48.0, 15
	8 April	05	05:44:17–05:53:55	03:39:45–05:56:60	0.2	5.6, 3.9	n/a, 142	40.3, 15
	17 April	11	05:38:11–05:49:45	04:41:46–07:13:15	0.1	4.4, 3.6	n/a, 74	39.8, 15
C-130, T. O.	4 April	03, 03	02:49:22–02:59:20	02:45:00–02:52:57	30[d]	20.1, 16.6	348, n/a	3204, 3167
			03:01:44–03:11:16	02:55:07–03:06:54		17.3, 22.2	350, n/a	2900, 2865
			03:14:46–03:28:30	03:14:09–03:23:58		17.4, 12.0	83, n/a	2299, 1960
			03:31:12–03:44:04	03:31:13–03:46:47		8.9, 13.6	170, n/a	1546, 1511
			03:46:56–04:01:56	03:56:05–04:03:16		2.6, 2.5	289, n/a	622, 600
			04:04:14–04:19:32	04:07:48–04:18:43		2.2, 4.1	268, n/a	50, 45
	27 April	15, 17	01:42:16–02:03:58	01:38:24–02:09:20	5[e]	1.1 n/a	105, n/a	156, 181
			02:12:42–02:35:42	02:11:42–03:12:14		1.7, n/a	138, n/a	457, 500
R. Brown, Gosan	16 April	n/a	06:30–10:30	11:57–15:58	150	7.6, 8.5	140, 153	15, 82[c]

[a]Wind data and sampling altitude are given for both platforms in the order given in column 1. "Distance" is the platform separation for the point at which they were in closest proximity. The wind direction and aircraft flight path direction (Figures 1–6) can be compared to see whether the aircraft was flying crosswind or along the wind.

[b]Note that the C-130 data show that the winds at the Gosan station were significantly affected by the island, as they were out of the east to the north and south of the island, but shifted northeast to southeast from the north end to the south end of the west coast of the island.

[c]The Gosan station is at 72 m altitude, and the optical sampling stack was 10m above the surface. Because air will be lifted as it passes over the island, the effective sampling height is probably closer to 10–20 m ASL.

[d]The C-130 and Twin Otter flew parallel stacked legs in a northwest-southeast direction on this day. The distance given here is their mean east-west separation. The flight tracks were both centered on the same latitude.

[e]The C-130 and Twin Otter flew parallel stacked legs in an east-west direction on this day. The distance given here is their mean north-south separation.

enough data for a meaningful comparison while optimizing our chances of having the aircraft and surface station measure similar air masses. Ideally, the aircraft fly-bys of Gosan and the Ron Brown would have been configured so that the aircraft started directly up- or down-wind of the surface platform then flew along the direction of the wind. In this configuration, the aircraft would fly through an air mass that was in the process of passing over the surface station so the two platforms could truly measure comparable air masses. Unfortunately the aircraft flight pattern was sometimes such that the wind was cross-track, so the two platforms were only sampling the same air when the aircraft was immediately up or downwind of Gosan or the Ron Brown (Figures 1–3).

[10] Even for cases where the air masses sampled by the two stations differ, it is optimal to compare data sets encompassing the same size volume of air. This allows us to make a meaningful comparison between the variability of optical parameters as well as their mean. Thus, having selected the segment of the aircraft leg that is within 35 km of the surface station, wind data at the surface station were used to calculate the sample period that covers an air mass equivalent to that covered by the aircraft sample. In cases where the wind was along the flight track the two

platforms measured the same air mass, separated only by the east-west distance between the two. When the air flow was cross-track, the sample period is calculated in the same way so that equivalent volume air masses were sampled, even if the same air mass could not be.

2.2. C-130/Gosan Fly-Bys

[11] The C-130 flew low-altitude legs past the Gosan surface station (33.2833N, 126.1667E) during five flights for a total of seven fly-bys, with two comparisons each on Research Flights (RF) #07 and #10 (Table 1). Due to air space restrictions, the C-130 had to follow a north-south path to the west of Jeju Island, so it was always closest to the station (within <5 km) when it was directly west of the island (Figure 1). The C-130 also sometimes flew an east-west leg starting just south of Jeju and heading westward, but these data are not included because the aircraft was always too far away from Gosan for a meaningful comparison.

[12] For four of the five fly-bys winds were out of the north/north-west/west, so air only passed a short distance over land before being sampled at the station (Figure 1). However, on the first fly-by (RF#04 on 06 April) the winds were out of the east so the air passed over the full width of
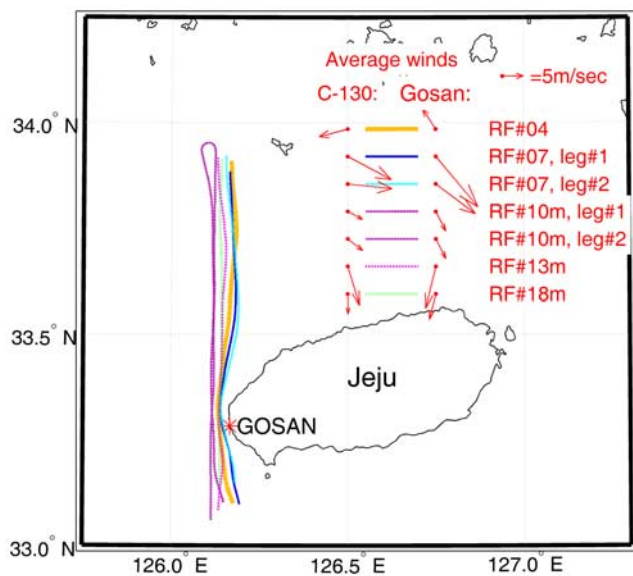
Figure 1. The C-130 flew seven low-altitude (<100 m) legs to the west of the Gosan surface station. The average wind direction and speed as measured from the C-130 and at Gosan during each comparison are indicated by the direction and length, respectively, of the arrows in the legend. Also shown is the length of an arrow corresponding to a wind speed of 5 m/sec. See color version of this figure at back of this issue.

Figure 2. As in Figure 1, but for the four C-130 fly-bys past the ship RV Ron Brown. The C-130 flight track and winds are shown in grey. The starting point of the grey arrows indicates the location of the RV Ron Brown, and the grey arrow the wind (direction and speed) on the Ron Brown.

the island before reaching Gosan. The wind data from the C-130 shows a significant island influence, with the wind coming out of the northeast north of the island and out of the southeast south of the island. This accounts for the difference between the C-130 and Gosan mean wind directions for this day (Figure 1).

2.3. C-130/Ron Brown Fly-Bys

[13] The C-130 flew low-altitude comparison legs that passed within 5 km of the NOAA ship RV Ron Brown on four of its 19 research flights (Table 1 and Figure 2). For all of these legs, the winds were blowing along or nearly along the C-130 flight path, although the wind shifted direction along the C-130 flight track for two of the comparisons (RF#03 and RF#09), possibly indicating a change in air mass.

[14] On RF#08, the C-130 flew an east-bound leg just north of the ship then turned and flew a short leg in a west/ northwest direction back towards the ship; only the first, longer leg is included in this comparison. On RF#09, three low-altitude legs were flown past the Ron Brown, all three oriented in a southwest/northeast direction. The last of these three legs is not included here because it is only three minutes long.

2.4. Twin Otter/Ron Brown Fly-Bys

[15] The Twin Otter did three flights past the Ron Brown, on 6 April (RF#04), 8 April (RF#05), and 17 April (RF#11) (Table 1 and Figure 3). Optical data are available for the Twin Otter for two of these (RF#04 and RF#11), both of which took place to the southeast of Jeju island. The aircraft passed within <0.4 km of the ship on each of the fly-bys, but followed a curved path for two of the flights so it is not
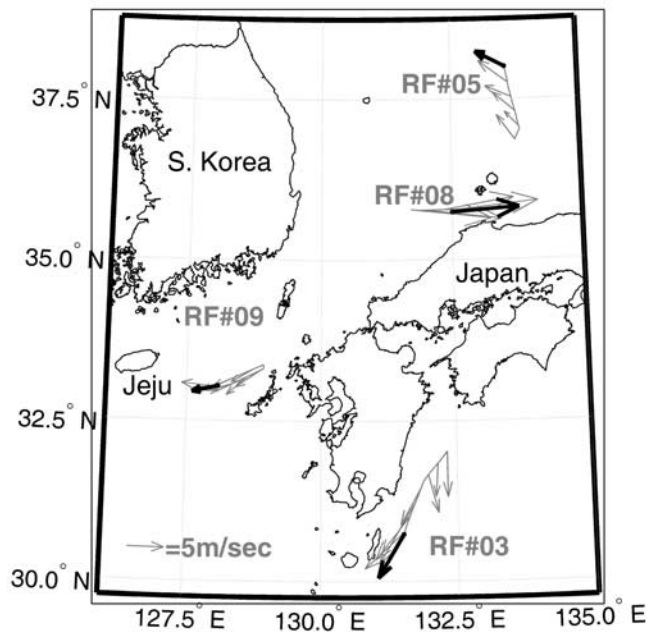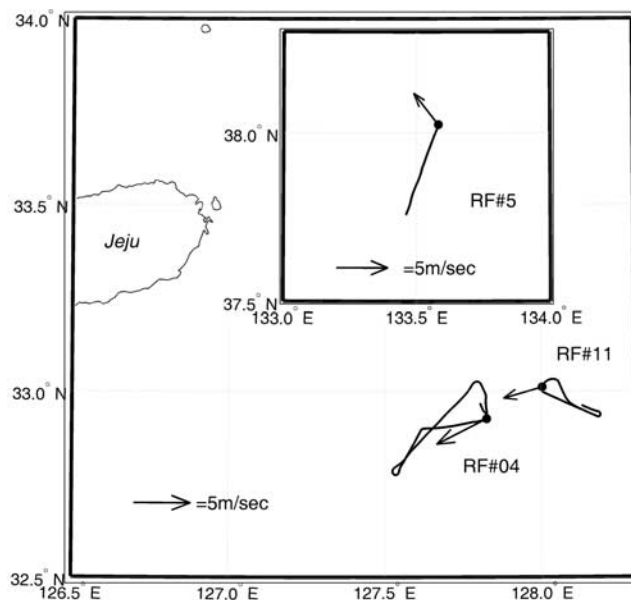

Figure 3. As in Figure 2, but for the Twin Otter flights past the Ron Brown. The fly-bys on RF#04 (06 April) and on RF#11 (17 April) were in the same vicinity, southeast of Jeju island. The fly-by on RF#05 (08 April) was northeast of this region, directly east of North Korea in the Sea of Japan (see Figure 6). The data from this day are shown in an inset box.
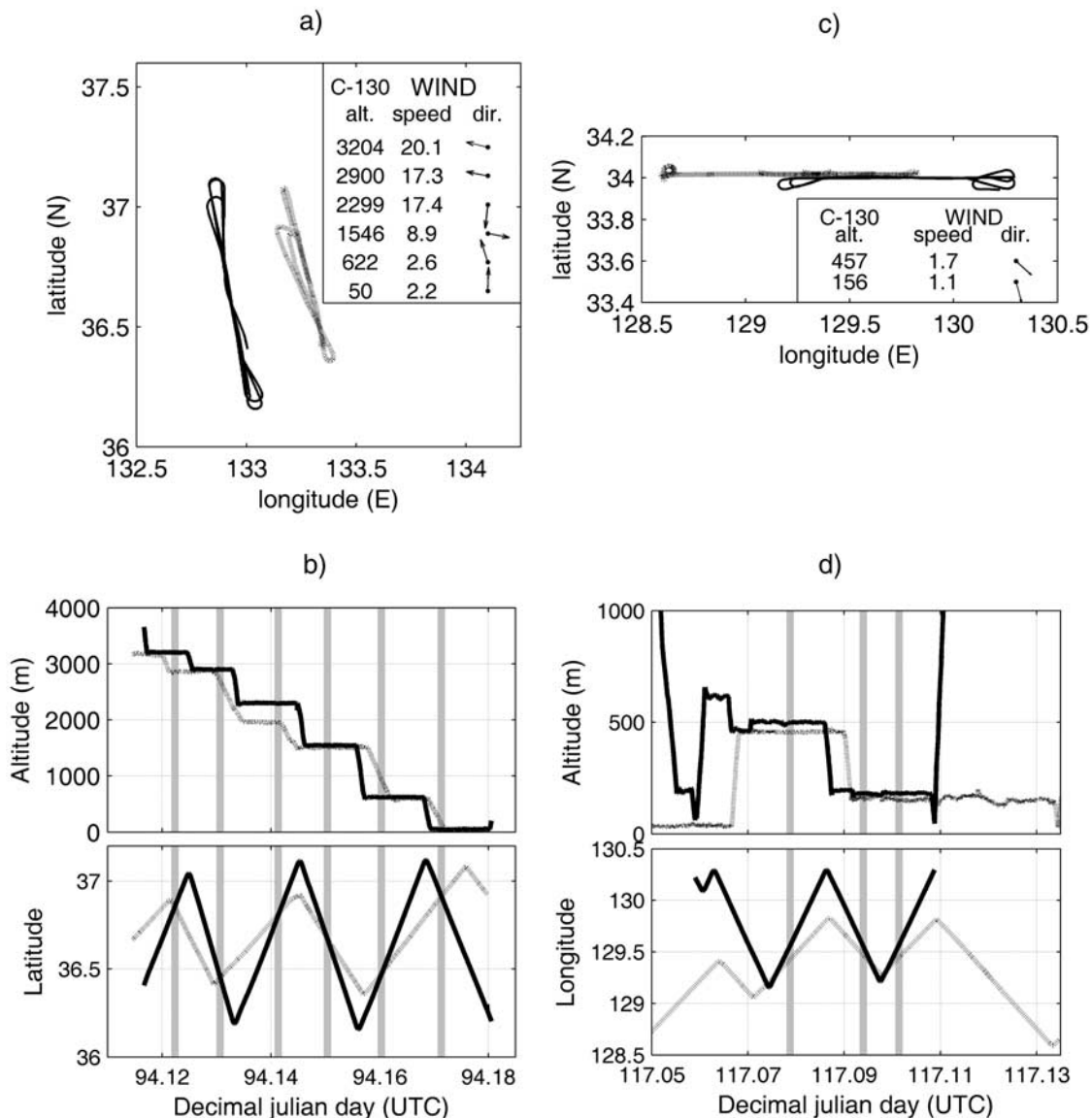
Figure 4. The C-130 and Twin Otter flew coordinated flights on (a and b) 04 April, which was RF#03 for both aircraft and on (c and d) 17 April, which was C-130 RF#15 and Twin Otter RF#17. The flight tracks of the C-130 (solid line) and Twin Otter (dotted line) are shown, along with the average wind speed and direction as measured from the C-130 on each of the six coordinated level legs (a, c). Both aircraft's flight patterns were nearly north-south in orientation on 04 April and east-west on 27 April, so we also show their latitude (c) or longitude (d) as a function of time. Times when the C-130 and Twin Otter were in closest proximity are indicated by grey lines in (b) and (d).

clear to what degree the platforms sampled similar air masses.

2.5. C-130/Twin Otter Coordinated Flights

[16] The C-130 and Twin Otter aircraft flew coordinated legs at a range of altitudes on two days (Figure 4), although optical data are only available for the Twin Otter on the second of these flights. Because the C-130 flies at about twice the speed of the Twin Otter, the two aircraft could not fly next to each other for the duration of the comparison and so were colocated at most twice during each leg.

[17] On 04 April, six stepped flight legs were flown in a nearly north-south orientation so the two aircraft were in

closest proximity when they were at a common latitude (Figures 4a and 4b). For five of the six legs the two aircraft were separated in altitude by <50 m, but for the leg at ∼2250 m the two were separated by ∼340 m altitude. However, this may not be a significant problem since both of these legs appeared to be within the same aerosol layer and at similar concentrations (Figure 5a). Also problematic is that either the two aircraft were at different altitudes (leg 3) or the Twin Otter was in the process of descending (legs 2, 5, and 6) when they were in closest lateral proximity. Finally, the two aircraft were separated in the east-west direction by ∼30 km so data from this day do not constitute a very robust comparison. In any case, optical data are not available for the Twin Otter.
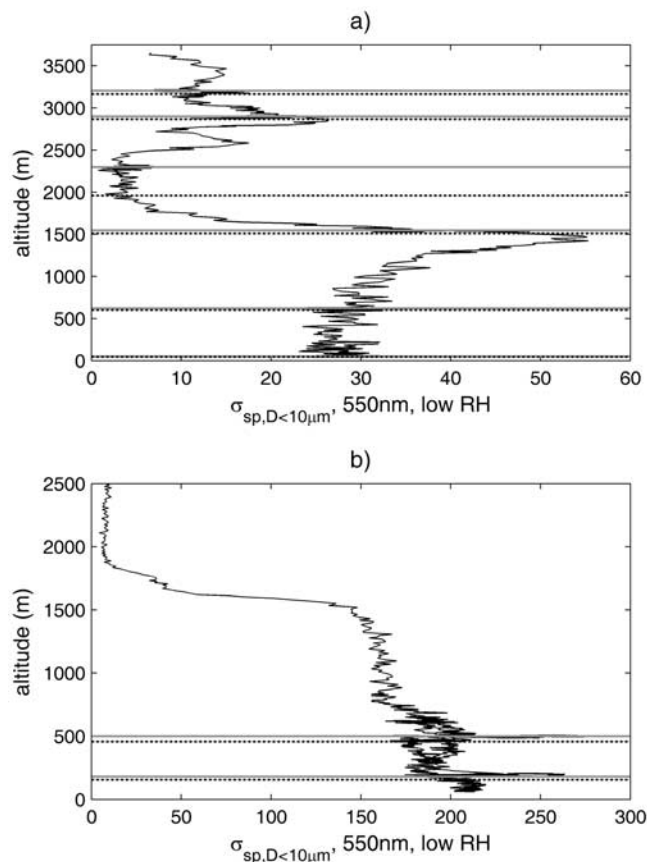
Figure 5. Low-RH light scattering (550 nm) as a function of altitude as measured from the C-130 during the C-130/ Twin Otter coordinated flights on (a) 04 April and (b) 27 April. The altitudes of the C-130 legs (solid lines) and Twin Otter legs (dotted lines) are also shown.

[18] On 27 April, a second set of coordinated legs was flown (Figures 4c, 4d, and 5b), this time along an east-west track. The north-south separation between the two aircraft during these legs was <5 km, and their altitude matched to within ~50 m. While the two aircraft both covered 129.25– 129.75° longitude, they usually were not at the same longitude at the same time. Because of this and because the wind was cross-track (Figure 4c) if there was a north-south gradient in the aerosol field we cannot expect the two measurements to agree for most of the leg. Thus the best comparison times were when both aircraft were at ~129.5° longitude at about the same time and both were flying level and straight (grey lines in Figure 4c).

2.6. Ron Brown/Gosan Comparison

[19] Due to navigational restrictions on the Ron Brown it never passed close to Jeju island. However, there is one time period when the Ron Brown was southeast of the island and the local winds on the ship and at Gosan, as well as backtrajectories (not shown), indicate that the two stations likely measured the same air mass (Table 1 and Figure 6). The two platforms were separated by ~150 km during this period, so this is clearly not as rigorous a test as the other comparisons presented here, where the minimum platform separation was often <5 km. In addition while the surface

winds were consistently out of the south/southeast during the selected period, there was a rapid shift in the trajectory from SE-bound to NW-bound just before the air reached the ship. This may correspond with mixing of this air with other air masses, possibly producing increased spatial variability in the aerosol field.

[20] For this comparison we selected a segment of the Ron Brown data when the surface winds were consistent in both speed and direction and were out of the southeast. The start and end points of the leg are chosen so that the surface winds are blowing directly from the ship towards Gosan at the central point in the leg. Based on the wind speeds measured at the ship, this air reached Gosan 5.2 hours after passing over the Ron Brown. The Gosan sample period thus follows the Ron Brown sample period by this amount of time.

2.7. C-130/TRACE-P P3-B Comparison

[21] The NASA-sponsored TRACE-P (TRansport And Chemical Evolution – Pacific [*Jacob et al.*, 2003]) campaign, which also studied Asian aerosol properties, imme-
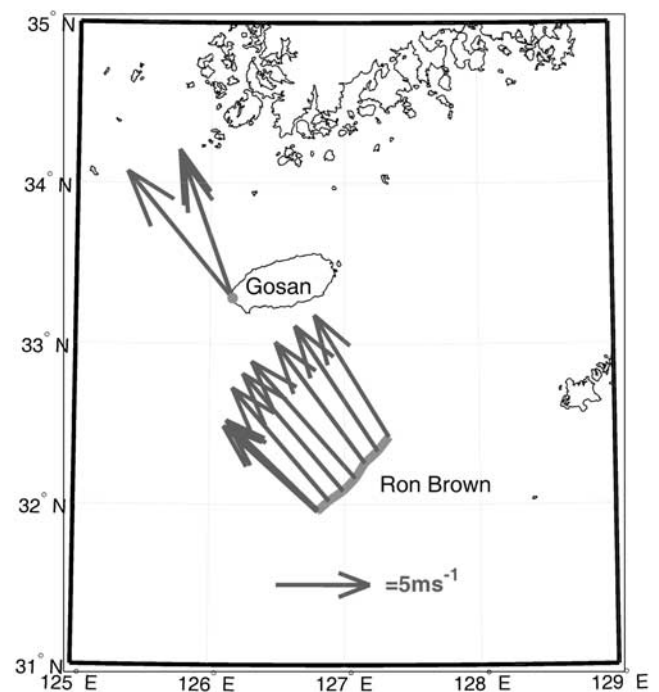

Figure 6. Shown are the surface winds as measured on board the Ron Brown and at the Gosan station for a time period when the two platforms' wind data and back trajectories from Gosan indicate that they measured similar air masses. Wind speed and direction are indicated by the arrows' length and direction, respectively, with an arrow length corresponding to 5 m/s shown for reference. The track of the ship during the period used in the comparison is shown as a lighter grey line and the location of the Gosan surface station as a lighter grey dot. Winds at Gosan are shown for a period of time that is the same length as that sampled on the Ron Brown (~4 hours), and during this period the winds at Gosan shifted from southeast (140°) to south-southeast (160°).
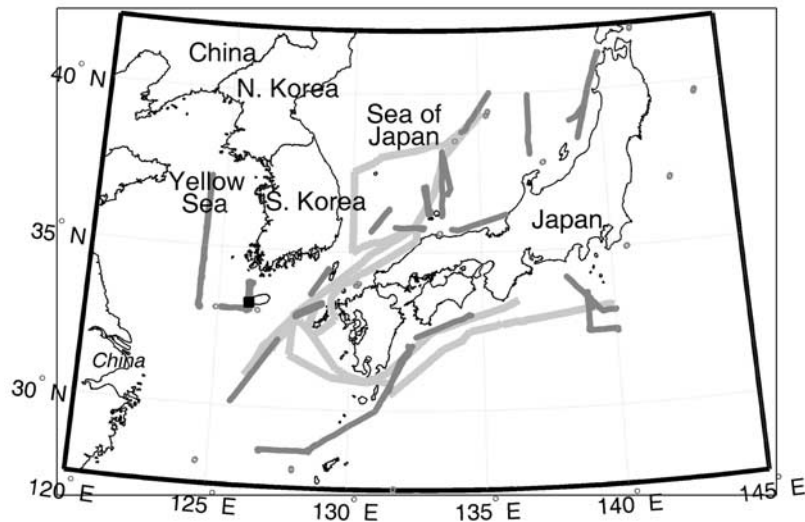
Figure 7. Shown are the platform locations for the data sets included in the ensemble comparison (Ron Brown, light gray; C-130 gray; Gosan, Jeju Island, black square at 33.283N, 126.167E).

diately preceded and overlapped with the ACE-Asia campaign. Similar in situ sets of measurements were made on the ACE-Asia NCAR C-130 and the TRACE-P NASA P-3B, so two wing-tip to wing-tip comparisons were flown between these aircraft. *Moore et al.* [2004] present the comparison of aerosol concentrations, size distributions, chemistry and optical properties. Thus we do not repeat the optical comparisons here but will cite their results in the context of identifying potential biases in the C-130 measurements.

3. Ensemble Comparison Data Sets

[22] In addition to comparing data from times when two platforms were roughly colocated, we also compare the campaign-wide data sets from the C-130, the Ron Brown and Gosan (Figure 7). Optical data for the Twin Otter was only processed for select time periods and so is not included in this part of the study. For the C-130, data from all 19 research flights (31 March to 04 May 2001, or days 90–124) are included in the analysis, but we only use data where the aircraft was flying <100 m altitude legs. The C-130 repeatedly flew L-shaped legs to the west of Jeju and north-south legs in the Yellow Sea (Figures 1 and 7), so there are actually data from several flights for each of these tracks. Ron Brown data from days 90.45–110.0 (31 March to 20 April) are included, as this is when the ship was in the ACE-Asia study region. Gosan data span the first day optical properties were measured through the day of the last C-130 flight (days 95.47–124.5).

[23] As can be seen in Figure 7, the Ron Brown and C-130 both covered regions off the south, west and north coasts of Japan, but the Ron Brown never went near Jeju Island or into the Yellow Sea. We will show later that the aerosol was considerably more dust-dominated in the Yellow Sea region than in the Sea of Japan or south of Japan so we expect the aerosol optical properties from these two regions to differ. Therefore a better comparison is between the Ron Brown and a subset of the C-130 data that does not include the Yellow Sea legs or the L-legs to the southwest of

Jeju. This subset of data set is referred to hereafter as "C-130, no Yellow Sea."

[24] Similarly, the Gosan data are from one location and so cannot be expected to compare well with the more geographically broad C-130 and Ron Brown data sets. Statistics were thus also calculated for a subset of the C-130 data containing only samples from the L-legs near Jeju and the North-South Yellow Sea legs (Figure 7). These can be compared to a subset of the Gosan data from only those times when the local winds were out of the west/ northwest – i.e. coming from the Yellow Sea region.

[25] In summary, the following data sets are included in the ensemble comparison: (1) C-130, all data; (2) C-130, no Yellow Sea or Gosan legs; (3) C-130, only Yellow Sea and Gosan legs; (4) Gosan, all data; (5) Gosan, winds 270–330°; (6) Ron Brown, all data. The data sets we expect to be most directly comparable are 2 versus 6 and 3 versus 5 (Figure 8). If the direct interplatform comparisons and these two "best-case" ensemble comparisons show good agreement, then we can interpret differences in "C-130, all data," "Gosan, all data," and "Ron Brown, all data" as real differences in the ambient aerosol sampled by these platforms.

4. Optical Properties

4.1. Measured Parameters: Extensive Properties

[26] Detailed descriptions of each platform's in situ optical measurements have been given elsewhere (C-130 [*Anderson et al.*, 2003], Ron Brown [*Quinn et al.*, 2004; *Carrico et al.*, 2003], Gosan [*Sheridan et al.*, 2001], Twin Otter [*Wang et al.*, 2002; *Schmid et al.*, 2003]) and so will not be repeated here. However, we will briefly highlight a few aspects that are directly relevant to the comparisons presented herein.

4.1.1. Measurements

[27] Low-RH total light scattering (σ_{sp}) and hemispheric backscattering (σ_{bsp}; i.e. 90°–180° scattering) were measured on all four platforms with TSI, Inc. model 3563 three-wavelength (450, 550, 700 nm) nephelometers and light absorption (σ_{ap}) was measured at 565 nm then adjusted to
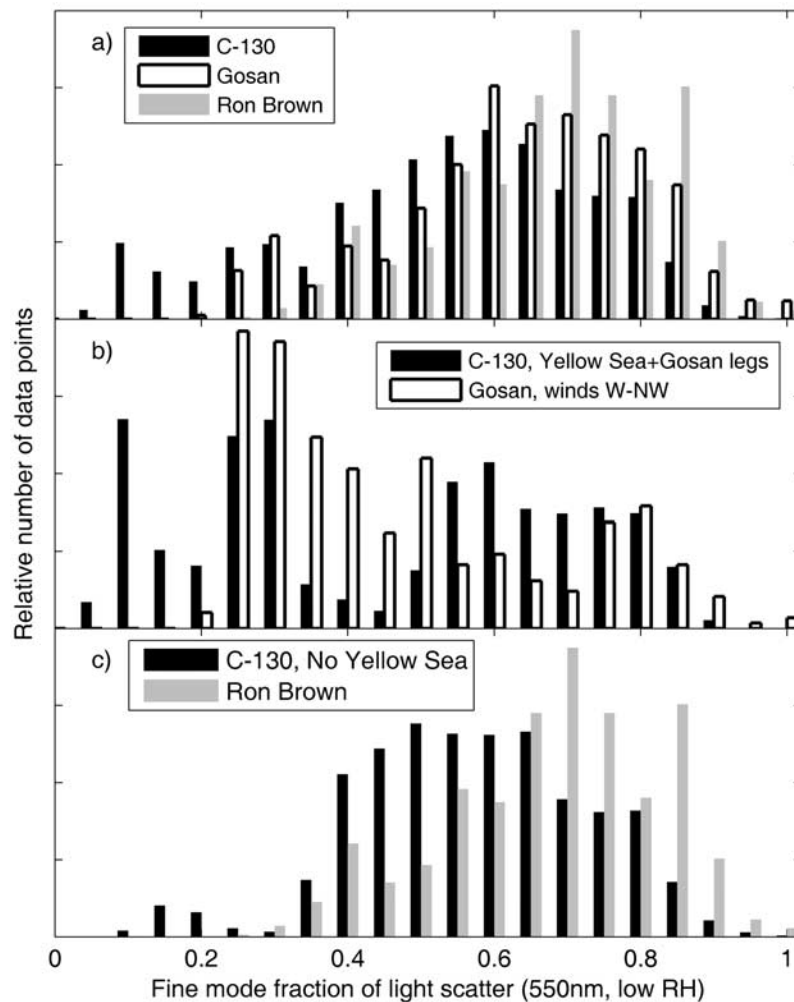
Figure 8. Differences in the aerosol sampled by the three platforms are reflected in histrograms of their aerosol fine mode fraction of light scattering for (a) their full data sets, as defined in section 3. The subsets of data expected to be most similar are (b) the "C-130, Yellow Sea + Kosan legs" and "Gosan, Winds W-NW" groupings and (c) the Ron Brown and the "C-130, No Yellow Sea" groupings.

550 nm per *Bond et al.* [1999] with Radiance Research Particle Soot Absorption Photometers (PSAPs). In addition light scattering hygroscopic growth, f(RH), was measured, as described in more detail below. All concentration-dependent parameters ("extensive properties") are given at standard temperature and pressure (273.2 K and 1013.2 mb).

[28] The TSI nephelometers on the Twin Otter suffered a series of instrumental problems that make the scattering data difficult to interpret and of questionable accuracy. Therefore the low-RH total light scattering values used here for the Twin Otter are from a low-RH Radiance Research model M903 nephelometer situated in the hygroscopic growth system. An important difference between the Radiance and TSI nephelometers is that the latter has been carefully studied so that correction factors needed to adjust the measured light scattering to σ_{sp} and σ_{bsp}, and the uncertainties in these adjustments, are well understood. Further, these correction factors have been shown to be consistent from instrument to instrument [*Anderson and Ogren*, 1998]. Such studies have not been done for the Radiance Research nephelometers. In particular, the sensitivity of the instrument to scattering at different angles, the range of angles over which scattering is

measured, and the wavelength dependence of the sensitivity have not been quantified.

[29] On all four platforms, calibration and performance checks were run throughout the campaign for all instruments (per *Anderson et al.* [1996], *Anderson and Ogren* [1998], and *Bond et al.* [1999]). Both the TSI, Inc. and Radiance Research nephelometers were calibrated using air and CO_2 before, during and after the campaign. All instruments were periodically switched to measuring filtered air so that instrumental noise could be determined under field conditions. On the C-130, because filtered air was measured at a range of altitudes we could also test for calibration changes under working conditions. These data revealed that rapid pressure and relative humidity changes can produce spurious data in the PSAP. (See *Anderson et al.* [2003] for further discussion.) In most cases, filters were changed on the PSAPs before the transmittance dropped below 0.7. Variations in the instruments' calibration and their noise levels are used to calculate the uncertainty in the measured parameters (section 4.5).

[30] In addition to recalibration, the PSAP data are adjusted for filter spot size, flow rate, and filter scattering

artefact (2% of scattering) as given by *Bond et al.* [1999], and the TSI, Inc. nephelometer data were adjusted for angular truncation using the procedure outlined by *Anderson and Ogren* [1998]. While the angular measurement range of the Radiance Research nephelometers has not been carefully quantified, cursory measurements on one M903 nephelometer indicate that the forward truncation angle is $\sim 11.5°$, which is considerably greater than the $\sim 7°$ forward truncation angle on the TSI nephelometer (N. Ahlquist, personal communication). It is not known whether this is typical of all M903 nephelometers. Nonetheless, the values of σ_{sp} shown here for the Twin Otter, which are from a Radiance Research nephelometer, have been corrected using the TSI, Inc. angular correction factors. In addition, based on the size distributions measured on the Twin Otter, an additional correction factor of $\sim 5 \pm 1\%$ of scattering was applied as a best-guess effort at compensating for the larger angular truncation in the Radiance nephelometer.

4.1.2. Relative Humidity Adjustments

[31] On the C-130, at Gosan and on the Twin Otter the "low-RH" measurements were made at $28.7 \pm 8.9\%$ RH, $33.8 \pm 7.6\%$ RH, and $\sim 30\%$ RH respectively, but on the Ron Brown they were made at $54.5 \pm 8.4\%$ RH. To make the data sets more comparable, for the direct interplatform comparisons between the C-130 and Ron Brown we have adjusted the C-130 values of σ_{sp} to the Ron Brown nephelometer sample volume RH using f(RH) values measured on the C-130 (see below) because the C-130 f(RH) values are available at the same time-resolution as are the dry light scattering values. For the Gosan/Ron Brown comparison, we have adjusted the Ron Brown values of σ_{sp} to the relative humidity in the Gosan nephelometer using growth as measured on the Ron Brown. For the ensemble comparison, all light scattering data are at low ($\sim 30\%$) RH. The hygroscopic growth behavior of light absorption was not measured and is not well understood, so no RH adjustments were made to the measured values of σ_{ap}.

4.1.3. Coarse/Fine Separation

[32] For the C-130, Ron Brown and Gosan, low-RH σ_{sp} and σ_{ap} were separately measured for the total and submicron aerosol. (Note that on the C-130 and Twin Otter, "total" aerosol refers to all aerosol passed through the inlet and sample plumbing. On the Ron Brown and at Gosan it refers to all aerosol that passed through a 10 μm diameter impactor.) The intention was to independently determine the optical properties of the fine- and coarse-mode aerosol, which are generally chemically distinct. On the C-130, total and submicron aerosol were measured simultaneously so $\sigma_{sp,D<10\mu m}$, $\sigma_{ap,D<1\mu m}$, $\sigma_{ap,D<10\mu m}$, and $\sigma_{ap,D<1\mu m}$, are all continuously available at 2 second resolution, except on RF#01–RF#05 when $\sigma_{ap,D<1\mu m}$ was not measured. Total and submicron aerosol were alternately measured every 15 minutes (for a 30 min. cycle) on the Ron Brown and every 7.5 minutes (for a 15 min. cycle) at Gosan, with data acquired at 1 min. resolution in both cases.

[33] On all three platforms the submicron separation was made using a Berner-style aerodynamic impactor [*Berner et al.*, 1979] run at ~ 30 lpm and employing a greased substrate to prevent particle bounce. This gives a 50% aerodynamic cutoff diameter (D_{aero}) of 1 μm and a 50% geometric cutoff diameter (D_g) of ~ 0.8 μm (for a density of 2.0 g·cm^{-3} and shape factor of 1.3). Size distribution

measurements show that the minima between the cross-sectional area size distributions falls between $D_g \sim 0.75$ μm and $D_g \sim 1.0$ μm and the minima in the volume size distributions falls between $D_g \sim 0.65$ μm and $D_g \sim 0.90$ μm so the $D_g = \sim 0.8$ μm cut point appears to be a good choice. A complicating factor is that the impactor was run at a different relative humidity on each platform: <40% on the C-130, $46 \pm 6\%$ at Gosan, and 55% on the Ron Brown. Hygroscopic growth will shift the aerosol to larger sizes, so the 1 μm cut point removes the most aerosol on the Ron Brown and the least on the C-130. On this basis alone, $\sigma_{sp,D<1\mu m}$ and $\sigma_{ap,D<1\mu m}$ should be lowest on the Ron Brown and highest on the C-130. We have not done anything to quantify or correct for this effect. An additional issue is that, for all of the impactors, the collection efficiency as a function of particle size is sigmoidal in shape. Thus, in cases where there is a significant coarse mode present, the "submicron" measurements may include the tail of the coarse mode aerosol. Similarly the D > 1 μm aerosol may include the upper tail of the fine mode.

4.1.4. Hygroscopic Growth Measurements

[34] On the C-130 and Twin Otter, f(RH) was measured with a pair of Radiance Research model M903 single-wavelength nephelometers running in parallel, one at low RH (nominally <40%) and one at high RH ($\sim 85\%$). This allowed for continuous measurement of f(RH), which is important on the aircraft since they cover a large spatial area in a short time. On the Ron Brown and at Gosan, f(RH) was measured with scanning-RH nephelometry systems (humidographs [*Carrico et al.*, 1998, 2000]). These systems include two 3-wavelength TSI 3563 nephelometers with a humidity control system between the two instruments. The first nephelometer, the dry reference nephelometer, was operated continuously at low RH (Ron Brown: $19 \pm 5\%$RH; Gosan: $35.3 \pm 7.5\%$RH). This was accomplished by additional sample heating (on the Ron Brown, to $33.5 \pm 1.9°C$; at Gosan, to $27.0 \pm 2.9°C$). An RH control system followed the first nephelometer and scanned the sample RH by adding water vapor and/or changing the temperature. Downstream of the RH controller, the scanning RH nephelometer measured light scattering properties while scanning RH from $\sim 40\%$ to $\sim 85\%$ (Ron Brown) or $\sim 90\%$ (Gosan). Here we use only the 550 nm total scatter data, as they are most directly comparable to the 540 nm total scatter f(RH) data from the C-130 and Twin Otter.

[35] On the Ron Brown and at Gosan, light scattering hygroscopic growth were alternately measured for the total and submicron aerosol, with the size cut made on the dried aerosol. At Gosan, during a single humidification cycle the measurements alternated between sub-10 μm and sub-1 μm aerodynamic every 6 minutes. A single humidification cycle occurred hourly and gave f(RH) for both the total and submicron aerosol. On the Ron Brown, a full humidogram (up- and down-scan in RH) was generated at one size cut then another was generated at the other size cut. The result is 55 minute resolution data that alternate give total f(RH) and submicron f(RH). The advantage to the Gosan approach is that data are available at both size cuts once per hour. However, because the data are not contiguous for a given cut size and because RH-scanning is only in the increasing direction, the data do not clearly yield information on whether the aerosol growth was deliquescent or monotonic.

[36] On the C-130, the default configuration for the f(RH) system was to measure total light scattering. However, at times the f(RH) system was manually switched to measuring only the submicron aerosol. This was usually done once during each interplatform comparison. The flow through the Radiance Research nephelometers is only 6 lpm, so a smaller, three jet, single stage impactor was used, making the cut on the dried aerosol. (The impactor jets were 1.1 mm diameter, and the jet plate distance was 0.075 mm. This design yields a 50% cut point of 1 μm when run at 5 lpm.) Unfortunately, the impactor was incorrectly installed for RF#09–RF#13, such that submicron f(RH) data from these flights is unavailable. On the Twin Otter, f(RH) was only measured for the total aerosol.

4.2. Derived Parameters: Intensive Properties

[37] Using the leg-averaged values of total and submicron light scattering ($\sigma_{sp,D<10\mu m}$ and $\sigma_{sp,D<1\mu m}$), hemispheric backscatter (σ_{bsp}), total and submicron light absorption ($\sigma_{ap,D<10\mu m}$ and $\sigma_{ap,D<1\mu m}$), and humidified light scattering, we derive several optical properties that will vary with aerosol type. Of interest is a) whether the optical properties of the different chemical components within the aerosols varied and b) how the optical properties of the entire aerosol mixture varied as a function of the component make-up. For the ACE-Asia aerosol, the fine mode aerosol was comprised predominantly of pollution and the coarse mode predominantly of dust and (at times) sea salt. Thus the ratio of D < 1 μm light scattering to total light scattering – the fine mode fraction of light scattering, FMF_{scat} – gives an indication of the relative amounts of pollution versus dust and/or sea salt in the sample:

$$FMF_{scat} \equiv \frac{\sigma_{sp,D<1\mu m}}{\sigma_{sp,D<10\mu m}}, \qquad (1)$$

FMF_{scat} is related to the fine mode-to-total aerosol mass ratio, which can be readily calculated in chemical transport models. Similarly, the Ångström exponent, defined as

$$\mathring{a}(\lambda_1/\lambda_2) \equiv -\log\left(\sigma_{sp,\lambda_1}/\sigma_{sp,\lambda_2}\right)\log(\lambda_1/\lambda_2), \qquad (2)$$

and calculated for (λ_1 = 450 nm, λ_2 = 550 nm) and (λ_1 = 450 nm, λ_2 = 700 nm), varies with aerosol size such that it is low ($\mathring{a} < \sim0.7$) when the aerosol is coarse mode dominated and high ($\mathring{a} > \sim1.5$) when it is fine-mode dominated. This parameter is also commonly calculated from satellite-based radiance measurements and so can be used to link in situ data to satellite data.

[38] The hemispheric backscatter fraction can be used to approximate the fraction of sunlight scattered back to space, or the upscatter fraction, and is calculated as:

$$b \equiv \sigma_{bsp}/\sigma_{sp}. \qquad (3)$$

Note that σ_{bsp} is only equal to upscatter fraction for a solar zenith angle of 0°. (See section 8 for further detail.) This parameter was measured on all platforms except the Twin Otter.

[39] A critical property of aerosols is the relative amount of light they scatter versus absorb, given by the single scatter albedo:

$$\omega \equiv \frac{\sigma_{sp}}{\sigma_{sp} + \sigma_{ap}} = \frac{\sigma_{sp}}{\sigma_{ep}}, \qquad (4)$$

where σ_{ep} is total light extinction. On the C-130 and the Ron Brown and at Gosan single scatter albedo is separately calculated for the total ($\omega_{D<10\mu m}$), submicron ($\omega_{D<1\mu m}$) and supermicron ($\omega_{D>1\mu m}$) aerosol, where $\omega_{D>1\mu m}$ is calculated using $\sigma_{sp,D<10\mu m} - \sigma_{sp,D<1\mu m}$ and $\sigma_{ap,D<10\mu m} - \sigma_{ap,D<1\mu m}$. On the Twin Otter, $\omega_{D<10\mu m}$ only is calculated. In all cases, ω is only given at 550 nm and at times when scattering is at least 10 Mm^{-1} to assure that enough aerosol is present for a meaningful measurement.

[40] The light scattering hygroscopic growth measurements are standardized by deriving a single parameter: f(RH)$_{40-85\%}$, the increase in light scattering for going from 40% to 85% RH. On the C-130 and Twin Otter, where scattering was measured at ~540 nm (see section 7) and only at two RH points (<~40%) and ~85%), f(RH) is assumed to follow the exponential form:

$$f(RH) = \left(\frac{100 - RH_{low}}{100 - RH_{high}}\right)^{\gamma}. \qquad (5)$$

The exponential γ is derived from the two-point data as:

$$\gamma = \frac{\ln\left(\sigma_{sp,lowRH}/\sigma_{sp,highRH}\right)}{\ln\left(\left(100 - RH_{high}\right)/\left(100 - RH_{low}\right)\right)}. \qquad (6)$$

Using γ, f(RH)$_{40-85\%}$ is calculated from equation (5). On the C-130, RH$_{low}$ was often <40%, but in equation (5) we fixed RH$_{low}$ at 40% when RH ≤40%, because the scanning-RH data on the ship showed that f(RH) is flat below 40%. This approach prevents us from under-estimating f(RH)$_{40-85\%}$ on the C-130 because we are using an approximate functional form for hygroscopic growth. At Gosan, the same functional form is used as given in equation (5), only γ is determined at 550 nm by minimizing the chi-squared error between the fit line and the σ_{sp} versus RH data points.

[41] On the Ron Brown, scattering was measured for both up-scans and down-scans in RH so a more sophisticated fitting approach is used, as described in detail by *Carrico et al.* [2003]. In brief, the measured f(RH) data were fit to either monotonic or deliquescent growth curves based on the observed curve structure, with separate fits for increasing and decreasing RH. Here, f(RH)$_{40-85\%}$ is derived for increasing RH, as the measurements on all platforms were made by first drying then humidifying the aerosol. Note that at Gosan and on the Ron Brown f(RH) was measured at 450, 550 and 700 nm, but here we only present the 550 nm data as it is most comparable to the C-130 and Twin Otter ~540 nm f(RH) data.

4.3. Data Resolution

[42] Because the C-130 and Twin Otter aircraft speeds are much greater than the surface wind speeds, the sampling periods for the aircraft (~5–10 min.) and surface stations (~2.5 hrs.) are quite different during the interplatform

comparisons (Table 1). Similarly, the aircraft data needs to be at much higher time resolution than the surface station data in order for their spatial resolution to be on a similar scale. In this study, we use 2 second averages for all of the C-130 data, which for typical airspeeds of ∼100 m/s corresponds to ∼200 m linear coverage per sample. As described below, the C-130 light absorption data have been smoothed over a 30 second window, but they are still given at 2 sec resolution, as are single scatter albedos calculated from the smoothed absorption data. This is done because the PSAP instrumental noise is ∼1.3 Mm^{-1} at this high a sample rate. The 30-second smoothing decreases the instrumental noise to ∼0.3 Mm^{-1}, levels comparable to that for the surface station measurements.

[43] The Twin Otter flew at ∼50−55 m/s during interplatform comparisons, so we have averaged this data to 4 seconds to also get ∼200−220 m linear coverage per sample. All Twin Otter optical parameters are at this time resolution.

[44] For Gosan low-RH scattering and absorption data are at 1 minute resolution, which for a wind speed of ∼5 m/s corresponds to ∼300 m linear coverage per sample. Aerosol hygroscopic growth is measured at one hour resolution. Total and submicron aerosol were alternately measured so FMF$_{scat}$ is at 12-minute resolution.

[45] On the Ron Brown, low-RH light scattering is at one minute resolution, again corresponding to ∼300 m linear coverage per sample assuming the ship is not moving and winds are ∼5 m/s. However, in this case the light absorption data are averaged over 30 minutes. The PSAP on the Ron Brown was run at ∼55−60% RH and it is now known that this instrument is more noisy when run at higher RH, so this averaging is necessary to reduce instrumental noise. As at Gosan, f(RH) was measured with a scanning-RH system so these data are at ∼55 min resolution.

[46] For a given comparison period, the variability of the optical properties will depend in part on the sampling frequency. Thus, based on the time-resolution of the data sets the most valid comparisons of variability will be between 1) low-RH total and submicron light scattering and Ångström exponents across all platforms and 2) light absorption and single scatter albedo on the C-130 versus that at Gosan.

4.4. Aerosol Sampling Efficiencies

[47] For the ACE-Asia measurements, sampling efficiencies were of particular concern for the in situ measurements because of the predominance of coarse mode dust. Coarse mode aerosol sampling is generally problematic on aircraft because of the high sampling velocity at the inlet. Thus, an inlet specially designed to efficiently sample large particles, the Low Turbulence Inlet (LTI [Lafleur, 1998]), was used on the C-130 aircraft. The LTI has sampling enhancements that increase with aerosol size so that efficiencies are much greater than one for supermicron aerosol. When combined with experimentally determined plumbing losses the system sampling efficiency is near unity for submicron aerosol, increases to >1.0 for aerosol up to ∼6 μm aerodynamic diameter, and drops off rapidly to near zero above ∼10 μm [Huebert et al., 2004; Anderson et al., 2003, Figure 4]. On the Twin Otter, a shrouded inlet was used which had a 50% aerodynamic cutoff diameter of 3.5 μm [Gao et al., 2003].

Plumbing losses between the inlet and the instruments were not quantified. On the ship Ron Brown, a mast-mounted inlet rotated to point into the wind to maintain isokinetic flow. Wind tunnel tests of this inlet yielded transmission efficiencies of >95% for particles of aerodynamic diameters up to 6.5 μm, which was the largest size tested [Bates et al., 2002]. A model of the Gosan inlet indicates that passing efficiencies were >∼95% up to ∼1 μm diameter, but efficiencies above this have not been carefully quantified. Plumbing losses also were not quantified for the surface stations. However, in all cases losses were minimized by using conductive tubing wherever possible and by minimizing the number of bends in the tubing [Bates et al., 2002; Anderson et al., 2003].

[48] Flow rates through all TSI, Inc. nephelometers was ∼30 lpm. Tests conducted on the C-130 [see Anderson et al., 2003, Figure 5a] indicate that losses within the TSI 3563 nephelometer were less than 1.5%, which is within the precision uncertainty of the instrument. (This result applies to the coarse-mode aerosol sampled in ACE-Asia, which was almost exclusively dust. A previous study on coarse-mode sea-salt aerosol [Anderson and Ogren, 1998] indicated somewhat larger losses.) The sample stream inside the PSAP makes several right-angle bends before reaching the sample filter, making particle losses a concern. The PSAPs used on the C-130 and the Ron Brown and at Gosan were modified so that most of the right angle bends were replaced with curved, conductive tubing. In all cases, the instruments were run at ≤1 lpm flow rate.

[49] Lab tests provide indirect evidence that coarse mode particle losses may not be significant in the PSAP at the flow rates used here. As documented by Bond et al. [1999], a 2% scattering correction must be applied to the measured value of absorption to account for multiple scattering of light within the instruments' sample filter. In a lab test, the PSAP was run with nonabsorbing coarse mode aerosol (zinc stearate), and application of the 2% scattering correction did not produce negative values of absorption, as would be the case if the particles were lost in the instrument plumbing (T. Anderson, personal communication). Nonetheless, rigorous tests are still needed to determine the passing efficiency of the PSAP plumbing, and we cannot yet rule out the possibility of significant losses and thus a low bias in σ$_{ap}$ and high bias in ω for coarse mode aerosol.

[50] At Gosan and on the Ron Brown, a 10 μm cut impactor was used upstream of all instruments to prevent insects and other large particles from being sampled. On the C-130, passing efficiencies were high for aerosol up to ∼10 μm diameter but dropped to near zero for particles larger than ∼12 μm [Anderson et al., 2003]. Finally, on the Twin Otter, no cut was actively applied for the total aerosol measurements, but the inlet passing efficiency is very likely near zero for D > 10 μm.

4.5. Means, Variability, Uncertainties, and Detection Limits

[51] For the direct interplatforms comparisons we show the means, coefficients of variation (standard deviation/mean), and uncertainties in the mean for the extensive (concentration-dependent) parameters. For the intensive properties we compare the means, standard deviations, and uncertainties. All uncertainties are for a 95% confidence

interval (C.I.). Coefficients of variation (COV) are not given for the intensive properties because a percentage change in the intensive properties in most cases is not meaningful when trying to relate that change to radiative forcing. For example, a 25% decrease in light scattering would translate directly into a 25% change in light extinction, but a 25% change in single scatter albedo – such as from 0.90 to 0.72 – could mean the difference between positive and negative top of the atmosphere forcing. Also, the Ångström exponent spans both negative and positive values (~-0.5 to $+3.0$) so a percentage difference (e.g. between å = −0.1 and å = +0.1) is not meaningful.

[52] The nephelometer and PSAP detection limits are twice their empirically determined noise level (i.e. signal standard deviation when measuring filtered air), which increases at higher sampling rates or resolution. For the highest resolution data (i.e. C-130), the detection limits are 0.6 Mm^{-1} for σ_{ap} (PSAP); 2.0 Mm^{-1} for 550 nm σ_{sp} (TSI nephelometer); and 1.0 Mm^{-1} for 550 nm σ_{bsp} (TSI nephelometer). An exception is the Twin Otter σ_{ap} data which have a detection limit of 3.0 Mm^{-1}. As will be seen later, aerosol concentrations for the data included herein were always high enough that these detection limits were exceeded.

[53] For the comparisons presented herein, scattering and absorption were universally measured using nephelometers and PSAPs. If we assume the two platforms being compared are sampling the same ambient aerosol and that both have the same sampling efficiencies the measured values of σ_{sp} and σ_{ap} should match within the instruments' *precision uncertainty*, or expected instrument-to-instrument variability. Therefore for the interplatform comparisons we test for agreement within the precision uncertainties. Also of interest is how well the measured values of σ_{sp} and σ_{ap} represent the real atmospheric aerosol (at low RH). This range is given by the instrument's *absolute uncertainty*, which is the precision uncertainty plus any potential discrepancy between what the instrument measures and the true ambient value. Here we only give the absolute uncertainties for the campaign-wide data sets (section 6), from which we reach conclusions about the mean aerosol properties in the ACE-Asia study region. Details on the derivation of precision and absolute uncertainty and their sensitivity to signal strength are given in previous studies [*Anderson and Ogren*, 1998; *Bond et al.*, 1999; *Masonis et al.*, 2002] and so will not be discussed herein. Note that we do not include corrections for or uncertainties in the sampling efficiencies in any of these calculations.

[54] Uncertainties in intensive properties are calculated directly from the uncertainties in the extensive properties, such that the uncertainty in intensive property X(y, z), δX, is given by

$$\delta X = \sqrt{\left(\frac{\partial X}{\partial y}\delta y\right)^2 + \left(\frac{\partial X}{\partial z}\delta z\right)^2}, \qquad (7)$$

where δy, δz are the uncertainties in the extensive properties y and z.

[55] In addition to calculating means, variability, and uncertainties, time-series of the data sets from each interplatform comparison were plotted and inspected for trends and/or anomalies. Because of the large number of direct interplatform comparisons these figures are not shown here, but we do discuss how trends affect the comparisons.

5. Comparison Results

[56] Insights into the source of discrepancies between any two platforms will be best made when viewed in the context of the full suite of direct interplatform comparisons. In this manner consistent biases or outliers will be more apparent. Thus we will start by reviewing the results of each interplatform comparison (sections 5.1–5.5) and the ensemble comparison (section 5.6) and then interpret the results collectively (section 6).

5.1. C-130 Versus Gosan

[57] Optical properties from the six times when the C-130 did fly-bys past the Gosan surface station are shown in Table 2. Total aerosol 550 nm light scattering and absorption values were consistently higher on the C-130 than at Gosan, the one exception being for $\sigma_{ap,D<10\mu m}$ on 02 May. The submicron aerosol discrepancies were much smaller than the total aerosol discrepancies, and for some legs $\sigma_{sp,D<1\mu m}$ was higher at Gosan. The discrepancies in σ_{sp} at 700 nm (18–50%; not shown) are considerably greater than those at 450 nm (7%–38%) or 550 nm (9–38%), though all are in the same direction (C-130 larger) and all exceed the $\sim$1–2% precision uncertainty of the scattering measurements.

[58] For all but the 06 April comparison the 550 nm $\sigma_{sp,D<10\mu m}$ discrepancies exceed the $\sigma_{sp,D<1\mu m}$ discrepancies, the difference being largest on 12 April which is the only comparisons where the aerosol was coarse mode dominated. Consistent with this result, å(450:700) was always lower on the C-130 and FMF$_{scat}$ was lower for all but one leg, when the winds were out of the east so the Gosan sample may include local island sources. This indicates that the C-130 sampled relatively more coarse mode aerosol than did Gosan. Higher values of [soluble Ca]:[SO$_4$] (an approximate proxy for the dust: pollution ratio) from the two comparisons where chemical data are available (12 and 18 April; data not shown) also imply that relatively more coarse mode aerosol was sampled on the aircraft. The higher FMF$_{scat}$ value from the C-130 on 06 April may be due to real differences in the ambient aerosol sampled by the two platforms. However, neither size distribution nor chemical data are available for 06 April and ω was not measured at Gosan on that day so we cannot tell whether this was the case.

[59] During the C-130 fly-bys past Gosan the hemispheric backscatter fraction (b) varied between $\sim$0.08 and 0.14. In all cases the Gosan values were higher than the C-130 values, generally by $\sim$0.02, which exceeds the precision uncertainty of the measurement. Note that an absolute difference of $\sim$0.02 constitutes about a 20% difference in the amount of light scattered into the backward hemisphere.

[60] For spherical aerosol, b is generally higher for fine-mode than for coarse-mode aerosol, so higher b at Gosan is consistent with the fact that higher FMF$_{scat}$ was measured at Gosan. Further, T-matrix calculations by *Kalashnikova and Sokolik* [2002] indicate that nonspherical sharp-edged aerosol have lower b than do volume-equivalent spherical par-

Table 2. Direct Interplatform Comparisons Between the C-130 and Gosan for Extensive Properties (All at 550 nm) and Intensive Properties[a]

Extensive Properties:	6-April-01 C-130 RF#04			12-April-01, Leg #1 C-130 RF#10			12-April-01, Leg #2 C-130 RF#10			18-April-01, N-Bound C-130 RF#13			18-April-01, S-Bound C-130 RF#13			2-May-01 C-130 RF#18		
	C-130	Gosan	Ratio	C-130	Gosan	Ratio	C-130	Gosan	Ratio	C-130	Gosan	Ratio	C-130	Gosan	Ratio	C-130	Gosan	Ratio
Ambient RH:	71.4	75.0	—	43.2	50.1	—	45.4	46.4	—	80.5	76.8	—	81.8	76.8	—	77.9	78.1	—
COV	4.1%	n/a	—	18.8%	n/a	—	10.6%	5.2%	—	1.9%	3.8%	—	2.8%	3.8%	—	3.9%	0.4%	—
Neph RH:	33.3	30.0	—	16.1	23.5	—	17.4	22.0	—	41.0	31.5	—	41.4	32.1	—	34.3	41.0	—
$\sigma_{sp,D<10\mu m}$:																		
Mean	84.82	77.28	1.10	293.5	213.2	1.38	218.39	181.23	1.21	85.18	77.06	1.11	86.27	77.55	1.11	135.95	124.80	1.09
COV	6.6%	3.5%		9.7%	7.1%		5.0%	10.2%		11.5%	4.6%		11.5%	4.5%		7.2%	5.8%	
Precision uncert.	1.1%	1.1%		1.0%	1.1%		1.0%	1.1%		1.2%	1.1%		1.2%	1.1%		1.0%	1.1%	
$\sigma_{sp,D<1\mu m}$:																		
Mean	59.40	47.67	1.25	69.6	71.9	0.97	59.83	67.69	0.88	51.33	48.02	1.07	52.00	48.44	1.07	116.83	108.76	1.07
COV	5.6%	12.2%		12.0%	5.3%		6.3%	5.5%		15.2%	6.7%		16.0%	6.3%		6.7%	5.1%	
Precision uncert.	1.8%	2.1%		1.8%	1.7%		1.8%	1.7%		1.9%	1.9%		1.9%	1.9%		1.7%	1.8%	
Total/submicron			0.89			1.48			1.40			1.05			1.04			1.03
σ_{bsp}:																		
Mean	8.14	7.88	1.03	33.22	27.92	1.19	25.71	24.67	1.04	9.57	10.10	0.95	9.70	10.13	0.96	10.97	12.60	0.87
COV	10.7%	8.4%		10.5%	5.5%		7.4%	7.4%		12.9%	5.3%		12.8%	5.0%		9.3%	6.1%	
Precision uncert.	3.7%	3.6%		1.4%	1.5%		1.6%	1.5%		3.1%	2.9%		3.1%	2.9%		2.8%	2.4%	
$\sigma_{ap,D<10\mu m}$:																		
Mean	11.53	n/a	n/a	24.83	19.86	1.25	24.03	21.36	1.13	13.72	12.69	1.08	13.74	12.69	1.08	13.13	13.75	0.95
COV	14.1%	n/a		12.1%	8.6%		10.4%	13.2%		11.5%	11.0%		12.8%	10.3%		6.9%	11.5%	
Precision uncert.	5.9%	n/a		5.8%	6.0%		5.7%	6.0%		5.8%	6.0%		5.7%	6.0%		5.8%	6.0%	
$\sigma_{ap,D<1\mu m}$:																		
Mean	n/a	n/a	n/a	15.78	15.20	1.04	14.61	16.37	0.89	11.58	10.96	1.06	12.03	10.87	1.11	12.41	13.39	0.93
COV	n/a	n/a		13.3%	11.6%		11.5%	17.5%		12.6%	15.9%		11.9%	14.6%		6.3%	13.1%	
Precision uncert.	n/a	n/a		5.8%	6.0%		5.8%	6.0%		5.8%	6.0%		5.7%	6.0%		5.8%	6.0%	
Total/submicron			n/a			1.20			1.27			1.02			0.97			1.02

Intensive Parameters:	6-April-01			12-April-01, Leg #1			12-April-01, Leg #2			18-April-01, N-Bound			18-April-01, S-Bound			2-May-01		
	C-130	Gosan	Diff	C-130	Gosan	Diff	C-130	Gosan	Diff	C-130	Gosan	Diff	C-130	Gosan	Diff	C-130	Gosan	Diff
b:																		
550 nm	0.096	0.102	-0.006	0.113	0.131	-0.018	0.118	0.136	-0.018	0.112	0.131	-0.019	0.112	0.131	-0.019	0.081	0.101	-0.020
Std deviation	0.010	0.004		0.007	0.004		0.008	0.004		0.011	0.004		0.010	0.004		0.006	0.003	
Precision uncert.	0.004	0.004		0.002	0.002		0.002	0.003		0.004	0.004		0.004	0.004		0.002	0.003	
å:																		
(450, 700) mean	1.43	1.61	-0.180	0.49	0.67	-0.180	0.62	0.78	-0.160	1.51	1.72	-0.210	1.52	1.72	-0.200	1.78	2.02	-0.240
Std deviation	0.04	0.04		0.02	0.04		0.03	0.04		0.04	0.05		0.04	0.05		0.04	0.03	
Precision uncert.	0.05	0.06		0.05	0.06		0.05	0.06		0.06	0.06		0.06	0.06		0.05	0.05	
(450, 550) mean	1.46	1.49	-0.030	0.48	0.46	0.020	0.65	0.62	0.030	1.50	1.59	-0.090	1.53	1.59	-0.060	1.67	1.75	-0.080
Std deviation	0.07	0.04		0.05	0.06		0.05	0.05		0.04	0.04		0.07	0.04		0.08	0.03	
Precision uncert.	0.09	0.10		0.08	0.10		0.09	0.09		0.10	0.10		0.10	0.10		0.08	0.09	
$f(RH)_{40-85\%}$:																		
D < 10 μm mean	1.99	n/a	n/a	1.47	2.23	-0.76	1.62	2.16	-0.54	1.78	2.72	-0.94	1.83	2.62	-0.79	1.82	2.37	-0.55
Std deviation	0.05	n/a		0.04	n/a		0.04	0.16		0.04	0.07		0.07	0.18		0.03	n/a	
D < 1 μm mean	n/a	n/a	n/a	n/a	2.25		1.98	2.16	1.09	n/a	2.53		n/a	2.53		n/a	2.31	
Std deviation	n/a	n/a		n/a	n/a		0.04	0.08		n/a	0.03		n/a	0.03		n/a	0.02	
ω:																		
D < 10 μm mean	0.880	n/a	n/a	0.922	0.915	0.007	0.901	0.895	0.006	0.861	0.859	0.002	0.863	0.859	0.004	0.912	0.901	0.011
Std deviation	0.015	n/a		0.003	0.006		0.006	0.007		0.006	0.012		0.006	0.011		0.003	0.007	
Precision uncert.	0.006	n/a		0.004	0.005		0.005	0.006		0.007	0.007		0.007	0.007		0.005	0.005	
D < 1 μm mean	n/a	n/a	n/a	0.815	0.825	-0.010	0.804	0.805	-0.001	0.816	0.814	0.002	0.812	0.817	-0.005	0.904	0.890	0.014

Table 2. (continued)

Intensive Parameters:	6-April-01			12-April-01, Leg #1			12-April-01, Leg #2			18-April-01, N-Bound			18-April-01, S-Bound			2-May-01		
	C-130	Gosan	Diff	C-130	Gosan	Diff	C-130	Gosan	Diff	C-130	Gosan	Diff	C-130	Gosan	Diff	C-130	Gosan	Diff
Std deviation	n/a	n/a		0.014	0.014		0.013	0.002		0.007	0.023		0.009	0.022		0.003	0.010	
Precision uncert.	n/a	n/a		0.003	0.005		0.004	0.006		0.008	0.009		0.008	0.009		0.007	0.008	
D > 1 μm mean	n/a	n/a	n/a	0.961	0.968	−0.007	0.944	0.958	−0.014	0.941	0.944	−0.003	0.952	0.941	0.011	0.964	0.978	−0.014
Std deviation	n/a	n/a		0.006	n/a		0.005	n/a		0.010	n/a		0.010	n/a		0.016	n/a	
Precision uncert.	n/a	n/a		0.007	0.010		0.009	0.013		0.027	0.031		0.028	0.031		0.051	0.069	
FMF_scat:																		
Mean	0.700	0.617	0.083	0.237	0.337	−0.100	0.274	0.374	−0.100	0.603	0.623	−0.021	0.603	0.625	−0.022	0.859	0.871	−0.012
Std deviation	0.036	0.048		0.012	0.015		0.014	0.023		0.038	0.021		0.043	0.019		0.031	0.017	
Precision uncert.	0.015	0.015		0.005	0.007		0.006	0.007		0.013	0.014		0.013	0.014		0.017	0.018	

aLeg-average means, precision uncertainties, and absolute uncertainties are given. Also shown are coefficients of variation, COV, (standard deviation/mean) for the intensive parameters and the standard deviations for the extensive parameters. Extensive properties are compared as ratios and the intensive properties as differences. Scattering values are all adjusted to the Gosan nephelometer RH but $\hat{a}$ and ω values are at the measurement (nephelometer) RH.

ticles. Given that our optical measurements were all made on dried aerosol, the discrepancies in b may be due to shape effects as well as size differences since, especially at low RH, the ACE-Asia coarse mode aerosol (i.e. dust and/or sea salt) are more nonspherical than are the fine mode aerosol.

[61] The C-130 and Gosan measurements of single scatter albedo for the total and D < 1 μm aerosol differed by less than 0.010 for all but one of the comparisons, and in most cases the discrepancies were less than or about equal to the precision uncertainty of the measurement. For $\omega_{D>1\mu m}$, discrepancies were less than 0.015 and they were always within the precision uncertainty of the measurement. Note that the relatively higher precision uncertainties in the supermicron ω values come about because $\sigma_{sp,D>1\mu m}$ and $\sigma_{ap,D>1\mu m}$ are derived by differencing the total and submicron values of σ_{sp} and σ_{ap} and therefore contain the uncertainties associated with both.

[62] All of the properties discussed so far were measured at low (<60%) relative humidity. In order to properly adjust light scattering to ambient relative humidity, we must be able to accurately measure light scattering hygroscopic growth. There were large differences in f(RH)$_{40-85\%}$ for the C-130 versus at Gosan, with the latter values 30−55% higher. Lower f(RH)$_{40-85\%}$ on the C-130 would be consistent with the lower values of FMF$_{scat}$ if the coarse mode is predominantly dust and the dust is not as hygroscopic as the fine mode pollution aerosol. Unfortunately, for most of the fly-bys chemical data are not available that allow us to reach conclusions about the coarse mode aerosol composition. Also, the C-130 and Gosan data give different answers as to whether the fine mode aerosol was significantly more hygroscopic than was the coarse mode (Table 2 and section 6). These f(RH) discrepancies are important because for three of the four comparison days the ambient RH was >70%, so even if we could put reasonable constraints on the dry aerosol light scattering there would be significant uncertainties in the ambient-RH light scattering.

[63] As discussed in section 2.2, on three of the four C-130/Gosan comparison days the wind had a significant east-west component and so was blowing cross-track to the C-130 flight path (Figure 1). The 02 May comparison leg is the only one where the winds were along the flight track. On the other days, gradients in the aerosol field could result in differences between the C-130 and Gosan-derived aerosol optical properties. We attempt to evaluate the significance of this effect on the extensive properties by generating linear fits to each of the two platforms' light scattering data sets (D < 10 μm and D < 1 μm) then normalizing the leg-average scattering to its value when the two platforms were in closest proximity. These "detrended" ratios of the C-130-vs-Gosan values of $\sigma_{sp,D<10\mu m}$ and $\sigma_{sp,D<1\mu m}$ are given in Table 3 along with the measured ratios. On 06 April and 02 May, aerosol gradients had little effect on the relative concentrations on the two platforms. However, for the 12 April and 18 April comparisons there were significant linear trends − in the north/south C-130 data in particular − that affect the scattering comparison. Accounting for this somewhat improves the $\sigma_{sp,D<10\mu m}$ comparison on the first leg on 12 April but makes the comparison of the second leg worse. Further, it produces a larger disagreement for $\sigma_{sp,D<1\mu m}$ on both the 12 April legs. Detrending improves the comparison in both total and submicron aerosol scattering on both of the 18 April legs.

Table 3. For the C-130/Gosan Comparisons, the Aircraft Flight Track Was North-South, but the Winds Had a Significant East-West Component on All Comparison Days but 02 May[a]

	06 April	12 April Leg#1	12 April Leg#2	18 April N-Bound	18 April S-Bound	02 May
Measured average FMF_{scat}	0.648	0.277	0.324	0.602	0.601	0.848
		Measured C-130/Gosan Ratios:				
$\sigma_{sp,D<10\mu m}$, 550 nm	1.10	1.38	1.21	1.11	1.11	1.09
$\sigma_{sp,D<1\mu m}$, 550 nm	1.25	0.97	0.88	1.07	1.07	1.07
Measured $D < 10\ \mu m$ *ratio*: $D < 1\ \mu m$ *ratio*	0.89	1.48	1.40	1.04	1.04	1.03
		Detrended C-130/Gosan Ratios:				
$\sigma_{sp,D<10\mu m}$, 550 nm	1.10	1.28	1.24	1.05	1.08	1.08
$\sigma_{sp,D<1\mu m}$, 550 nm	1.23	0.92	0.87	0.99	1.03	1.07
Detrended $D < 10\ \mu m$ *ratio*: $D < 1\ \mu m$ *ratio*	0.89	1.40	1.43	1.05	1.05	1.01

[a]Real gradients in the aerosol field will thus not be equally sampled by the two platforms and will result in discrepancies in the measured optical properties. While there were no significant trends in the aerosol intensive properties during these comparison legs, there were gradients in the aerosol concentration. Here we have accounted for this effect and show the resulting ratio of C-130:Gosan total and submicron light scattering. The ratio between the total aerosol and submicron aerosol discrepancies and FMF_{scat} (which is the average of the C-130 and Gosan values) is also shown as an indicator of a size-dependent bias.

[64] We also tested whether gradients in the aerosol fields had an impact on the comparisons of the aerosol intensive properties – i.e., whether the aerosol type as well as concentration changed during the sample periods. In all cases these gradients were small enough that they are not worth accounting for. For example, adjustments for gradients in FMF_{scat} were always less than 0.01.

5.2. C-130 Versus Ron Brown

[65] As with the C-130/Gosan comparisons, total aerosol light scattering values are higher on the C-130 than on the Ron Brown (for all but the 17 April comparison; Table 4), and the ratio C-130:Ron Brown of $\sigma_{sp,D<10\mu m}$ is again always larger than the ratio of C-130:Ron Brown $\sigma_{sp,D<1\mu m}$. Here FMF_{scat} was always greater than 0.5 so we do not have a coarse-mode-dominated case with which we can test for a size-dependence to the discrepancies. What we can say is that the total- *versus* submicron scattering biases are not a function of FMF_{scat} for $FMF_{scat} > 0.5$. In all cases the scattering discrepancies were greater than the ~1–2% precision uncertainty of the measurements. However, here the discrepancies in scattering at 450, 550 and 700 nm are similar (not shown), whereas for the C-130 versus Gosan the 700 nm discrepancies were considerably larger.

[66] While FMF_{scat} is always higher on the Ron Brown, the discrepancies in å were in both directions and in most cases were within the precision uncertainty of the measurement. On the Ron Brown, å is calculated at ~55% RH, whereas on the C-130 it is at low (<40%) RH. Similarly, the impactor cut point is at a higher RH on the Ron Brown. Accounting for these differences in the Ron Brown data would lead to both higher FMF_{scat} and higher å, increasing the FMF_{scat} discrepancies and producing higher values of å on the ship.

[67] Both FMF_{scat} and å are functions of aerosol size so we would expect them to indicate similar differences between the two platforms, which they do not. The reason for this is not understood. The chemical data (not shown; available for all but 08 April) give much higher ratios of [soluble Ca]:[SO₄] (i.e. dust: pollution) and [Na]:[NssSO4] (i.e., sea salt: pollution) for the C-130 than for the Ron

Brown, which is consistent with the lower values of FMF_{scat} on the C-130 but not with the nearly equal values of å on the two platforms. (NssSO₄ = non-sea-salt sulfate.)

[68] Hemispheric backscatter fraction, b, is significantly lower on the C-130, with the differences (~0.02–0.03) about three to four times the precision uncertainty of the measurement and ~20–30% of the mean. Again this is consistent (according to model calculations) with relatively more coarse mode aerosol being sampled by the C-130 instruments.

[69] For most of the comparisons ω agrees to within 0.015, with two outstanding exceptions. First, on 04 April, $\omega_{D<10\mu m}$ is 0.077 lower on the Ron Brown, but because $\sigma_{apD<1\mu m}$ was not measured on the C-130 we cannot tell if the relatively higher $\omega_{D<10\mu m}$ is due to a difference in the coarse or fine-mode aerosol. Filter samples from this period show much higher ratios of [soluble Ca]:[SO₄] and [Na]:[NssSO₄] on the C-130, indicating relatively more dust and more sea salt. This is consistent with the observed higher $\omega_{D<10\mu m}$. However, the size distribution data (not shown) indicate that similar amounts of fine- and coarse-mode aerosol were present on the two platforms. Also, the chemical data also indicate much higher fractions of dust and sea salt on the other comparison days, and the discrepancies in $\omega_{D<10\mu m}$ and $\omega_{D>1\mu m}$ on these days are not nearly as large.

[70] Second, for the NE-bound comparison leg on 17 April there are large differences for both $\omega_{D<10\mu m}$ (0.032) and $\omega_{D>1\mu m}$(0.100), while $\omega_{D<1\mu m}$ agrees well (−0.003). On the SW-bound leg immediately following, ω agrees well for all three size cuts. Several factors may be at play here. FMF_{scat} was high on this day, so only ~10–15 Mm^{-1} of the scattering and <1.5 Mm^{-1} of the absorption was due to the coarse mode aerosol. These small signals lead to a large uncertainty in $\omega_{D>1\mu m}$ (~0.04), which nonetheless may be under-estimated. Also, time series of the data from the 17 April legs show that ω_{tot} was highly variable. During the comparison legs the wind direction shifted sharply on both platforms. This change in wind direction may be accompanied by a shift in air mass origin that is not sampled equally by the two platforms: i.e., $\omega_{D<10\mu m}$ is nearly the

Table 4. As in Table 2, but for the C-130/Ron Brown Comparison Legs[a]

Extensive Parameters:	4-April-01 C-130 RF#03			8-April-01 C-130 RF#05			13-April-01, E-Bound C-130 RF#08			17-April-01, NE-Bound C-130 RF#09			17-April-01, SW-Bound C-130 RF#09		
	C-130	R Brn	Ratio	C-130	R Brn	Ratio	C-130	R Brn	Ratio	C-130	R Brn	Ratio	C-130	R Brn	Ratio
Ambient RH	52.5	55.6	—	83.3	93.3	—	46.3	51.7	—	56.6	71.7	—	54.7	68.5	—
Covariance	3.6%	2.3%		2.0%	1.4%		4.5%	1.7%		3.5%	3.6%		5.9%	3.4%	
Neph RH	25.9	51.7	—	31.6	57.2	—	17.5	41.2	—	36.8	59.6	—	35.9	58.6	—
$\sigma_{sp,D<10\mu m}$:															
Mean	59.26	51.04	1.16	117.80	87.75	1.34	125.57	98.72	1.27	55.05	56.58	0.97	51.52	49.95	1.03
COV	5.8%	3.8%		3.7%	5.9%		4.5%	3.0%		8.6%	11.0%		11.1%	11.1%	
Precision uncert.	1.0%	1.2%		0.9%	1.1%		1.0%	1.1%		1.1%	1.1%		1.1%	1.2%	
$\sigma_{sp,D<1\mu m}$:															
Mean	30.54	28.29	1.08	85.12	65.11	1.31	65.11	57.00	1.14	38.77	45.06	0.86	35.62	40.74	0.87
COV	5.7%	4.1%		3.4%	10.6%		4.5%	3.1%		8.7%	11.2%		11.4%	11.3%	
Precision uncert.	1.6%	1.7%		1.7%	2.1%		1.6%	1.8%		1.5%	1.4%		1.5%	1.4%	
Total/submicron			1.10			1.05			1.16			1.15			1.19
σ_{bsp}:															
Mean	5.18	5.39	0.96	10.35	9.75	1.06	14.04	12.73	1.10	5.33	7.09	0.75	4.98	6.37	0.78
COV	14.5%	6.3%		8.2%	8.5%		8.5%	3.9%		15.6%	12.0%		18.5%	10.7%	
Precision uncert.	5.6%	5.2%		3.1%	3.0%		2.4%	2.4%		5.6%	3.9%		5.8%	4.4%	
$\sigma_{ap,D<10\mu m}$:															
Mean	4.82	7.33	0.66	16.09	8.63	1.86	12.21	9.02	1.35	7.68	8.37	0.92	7.38	7.09	1.04
COV	5.4%	12.6%		7.5%	10.9%		2.4%	4.4%		10.4%	21.0%		19.5%	7.5%	
Precision uncert.	6.8%	6.0%		5.8%	6.0%		5.9%	6.0%		6.3%	5.7%		6.1%	6.1%	
$\sigma_{ap,D<1\mu m}$:															
Mean	n/a	6.17	n/a	n/a	8.62	n/a	10.63	7.71	1.38	7.41	6.96	1.06	6.58	6.46	1.02
COV	n/a	3.4%		n/a	11.8%		2.5%	2.2%		9.2%	11.1%		22.0%	0.12	
Precision uncert.	n/a	6.0%		n/a	6.0%		5.9%	6.0%		6.2%	5.0%		6.1%	6.0%	
Total/submicron			n/a			n/a			0.98			0.87			1.02

Intensive Parameters	4-April-01			8-April-01			13-April-01, N-Bound			17-April-01, NE-Bound			17-April-01, SW-Bound		
	C-130	R Brn	Diff	C-130	R Brn	Diff	C-130	R Brn	Diff	C-130	R Brn	Diff	C-130	R Brn	Diff
b:															
550 nm	0.088	0.106	−0.018	0.088	0.111	−0.023	0.112	0.129	−0.017	0.097	0.125	−0.028	0.097	0.128	−0.031
Std deviation	0.014	0.008		0.007	0.006		0.010	0.004		0.015	0.008		0.016	0.008	
Precision uncert.	0.005	0.006		0.003	0.004		0.003	0.003		0.006	0.005		0.006	0.006	
å:															
(450, 700) mean	1.05	1.06	−0.010	1.57	1.46	0.110	0.97	1.07	−0.100	1.68	1.66	0.020	1.64	1.66	−0.020
Std deviation	0.06	0.09		0.06	0.09		0.04	0.05		0.07	0.07		0.07	0.07	
Precision uncert.	0.05	0.05		0.04	0.05		0.05	0.05		0.05	0.05		0.05	0.05	
(450, 550) mean	1.12	1.19	−0.070	1.60	1.57	0.030	1.07	1.19	−0.120	1.69	1.76	−0.070	1.62	1.77	−0.150
Std deviation	0.11	0.13		0.09	0.08		0.08	0.06		0.12	0.08		0.13	0.08	
Precision uncert.	0.09	0.10		0.08	0.09		0.08	0.09		0.09	0.09		0.09	0.09	
$f(RH)_{40-85\%}$:															
D < 10 μm *mean*	2.03	2.28*	−0.25	1.87	2.34	−0.47	1.60	1.84	−0.24	1.76	2.45	−0.69	1.80	2.43	−0.630
Std deviation	0.08	n/a		0.04	n/a		0.04	n/a		0.05	n/a		0.08	n/a	
D < 1 μm *mean*	n/a	2.65	—	n/a	2.38	—	1.73	2.22	−0.49	n/a	2.65	—	n/a	2.59	—
Std deviation	n/a	n/a		n/a	n/a		0.04	n/a		n/a	n/a		n/a	n/a	
ω:															
D < 10 μm *mean*	0.925	0.848	0.077	0.880	0.885	−0.005	0.911	0.899	0.011	0.878	0.846	0.032	0.875	0.858	0.017
Std deviation	0.007	n/a		0.008	n/a		0.005	n/a		0.016	n/a		0.021	n/a	
Precision uncert.	0.005	0.007		0.006	0.005		0.005	0.005		0.007	0.007		0.007	0.007	
D < 1 μm *mean*	n/a	0.778	n/a	n/a	0.860	n/a	0.860	0.863	−0.003	0.840	0.843	−0.003	0.844	0.829	0.015
Std deviation	n/a	n/a		n/a	n/a		0.007	n/a		0.012	n/a		0.023	n/a	
Precision uncert.	n/a	0.007		n/a	0.007		0.005	0.005		0.009	0.007		0.009	0.008	
D > 1 μm *mean*	n/a	0.943	n/a	n/a	0.968	n/a	0.975	0.960	0.015	0.984	0.884	0.100	0.952	0.942	0.010
Std deviation	n/a	n/a		n/a	n/a		0.007	n/a		0.036	n/a		0.030	n/a	
Precision uncert.	n/a	0.023		n/a	0.032		0.015	0.016		0.040	0.042		0.034	0.055	
FMF$_{scat}$:															
Mean	0.515	0.554	−0.039	0.723	0.742	−0.019	0.519	0.577	−0.059	0.704	0.796	−0.092	0.691	0.816	−0.124
Std deviation	0.044	0.039		0.035	0.037		0.030	0.015		0.056	0.028		0.058	0.118	
Precision uncert.	0.010	0.011		0.014	0.018		0.010	0.012		0.013	0.015		0.013	0.015	

[a]Here σ_{sp} values have been adjusted to the Ron Brown nephelometer RH, å is at the measured (nephelometer) RH for each platform, and ω is calculated from scattering values adjusted to the C-130 nephelometer relative humidity (i.e. low RH).

same for the two C-130 legs, whereas on the Ron Brown it is 0.013 lower on the first leg than on the second.

[71] Finally, light scattering hygroscopic growth is 12–40% higher on the Ron Brown than on the C-130. Recall that the C-130 values were also low compared to those from Gosan, only in that case the discrepancies were even larger.

Here the discrepancies in $f(RH)_{40-85\%}$ appear to increase with FMF$_{scat}$ though this correlation is by no means statistically robust.

[72] The comparisons shown in Table 4 are for C-130 and Ron Brown leg averages, and in cases where the winds did not follow the C-130 flight track (Figure 2) some of the

Table 5. As in Table 3, but for the C-130/Ron Brown Comparisons

	04 April	08 April	13 April	17 April Leg #1	17 April Leg #2
Average **FMF**$_{scat}$	0.536	0.739	0.543	0.723	0.738
		Measured C-130/Ron Brown Ratios:			
$\sigma_{sp,D<10\mu m}$, 550 nm	1.16	1.34	1.27	0.97	1.03
$\sigma_{sp,D<1\mu m}$, 550 nm	1.08	1.31	1.14	0.86	0.87
D < 10 μm ratio: D < 1 μm ratio	*1.09*	*1.05*	*1.16*	*1.15*	*1.19*
		Detrended C-130/Ron Brown Ratios:			
$\sigma_{sp,D<10\mu m}$, 550 nm	1.18	1.20	1.26	1.21	1.07
$\sigma_{sp,D<1\mu m}$, 550 nm	1.07	1.14	1.13	1.05	0.89
D < 10 μm ratio: D < 1 μm ratio	*1.08*	*0.99*	*1.04*	*1.25*	*1.22*

discrepancy may be due to horizontal gradients in the aerosol field. Thus we also compare $\sigma_{sp,D<10\mu m}$ and $\sigma_{sp,D<1\mu m}$ using the detrending and normalization method described in the previous section for the C-130/Gosan comparisons (Table 5). The results for 04 April (RF#03) and 13 April (RF#08) are essentially unchanged when gradients are accounted for. However, on 08 April there were ~20% gradients in $\sigma_{sp,D<1\mu m}$ and $\sigma_{sp,D<10\mu m}$ on the Ron Brown, and adjusting for this leads to significant improvements in both comparisons. There were also significant gradients measured on the Ron Brown on the first comparison leg on 17 April, but not on the second leg. The detrended comparison shows better agreement for $\sigma_{sp,D<1\mu m}$ but worse agreement for $\sigma_{sp,D<10\mu m}$, again indicating that the two platforms may have sampled characteristically different aerosol for at least part of this leg. Also for both of the 17 April legs the C-130 and Ron Brown concentrations were highly variable so applying a correction based on a linear gradient cannot be expected to properly compensate for the observed differences.

5.3. Twin Otter Versus Ron Brown

[73] Comparisons of total aerosol scattering, absorption, f(RH)$_{40-85\%}$ and single scatter albedo at 550 nm are for the two days when the Twin Otter flew past the Ron Brown are given in Table 6. Scattering on the Twin Otter was measured with Radiance Research nephelometers,

and uncertainties have not been quantified for these instruments, so we only show the means and variability of the measured parameters. On the 17 April fly-by, the light absorption data on the Twin Otter was extremely erratic and had to be manually filtered for obvious spikes and dropouts in the data. A single average value of single scatter albedo was therefore calculated for the leg and the variability in ω is not available. For both comparisons, scattering was higher (by 5% and 20%) on the Ron Brown than on the Twin Otter but light absorption was a factor of two lower. As a result the single scatter albedo is much lower on the Twin Otter. Note also that scattering and – more so – absorption are a factor of two to three more variable on the Twin Otter. Because the aerosol was fine mode dominated (FMF$_{scat}$ > 0.7), and because the discrepancies in σ_{sp} and σ_{ap} are of opposite sign, it is unlikely that the difference in ω is due to inlet sampling efficiency differences. Data on relative concentrations of black carbon are not available for the Twin Otter, so we cannot use chemical data to infer whether this discrepancy is real or a measurement artefact.

[74] Light scattering hygroscopic growth was also much lower on the Twin Otter than on the Ron Brown. Note that these discrepancies are similar in magnitude to those between the C-130 and Ron Brown and that on both the C-130 and Twin Otter f(RH)$_{40-85\%}$ was measured with a two-point system employing Radiance Research

Table 6. Shown is a Summary of the Two Direct Interplatform Comparisons Between the Twin Otter and the Ron Brown[a]

Extensive Parameters:	6-April-01			17-April-01		
	R Brn	T.O.	*Ratio*	R Brn	T.O.	*Ratio*
Ambient RH	65.4	65.0		70.3	63.5	
Nephelometer RH	55.1	<30%		58.8	<30%	
$\sigma_{sp,D<10\mu m}$, 550 nm	112.05	106.30	1.05	53.13	44.37	1.20
COV	*3.2%*	*5.6%*		*6.2%*	*11.2%*	
$\sigma_{ap,D<10\mu m}$, 550 nm	6.06	12.03	0.50	7.40	14.20	0.52
COV	*10.1%*	*31.0%*		*5.8%*	*11.3%*	

Intensive Parameters:	6-April-01			17-April-01		
	R Brn	T.O.	*Diff*	R Brn	T.O.	*Diff*
f(RH)$_{40-85\%}$	2.70	1.84	0.86	2.55	1.62	0.93
Std deviation	*n/a*	*0.90*		*n/a*	*0.04*	
ω, total aerosol	0.930	0.898	0.032	0.847	0.760	0.087
Std deviation	*0.006*	*0.030*		*n/a*	*0.00*	
FMF$_{scat}$	0.722	—		0.792	—	
Std deviation	*0.024*	—		*0.039*	—	

[a]Scattering values are all adjusted to the Ron Brown nephelometer RH, and single scatter albedo data are given for RH = 30% (Ron Brown) and RH < 30% (Twin Otter). FMF$_{scat}$ as measured on the Ron Brown is given to show that for both comparisons the aerosol was mixed to fine mode dominated.

Table 7. Comparisons for the Two Coordinated Legs That the C-130 and Twin Otter Flew on 27 April[a]

Extensive Parameters:	27-April-01, Leg #1			27-April-01, Leg #2		
	C-130	T.O.	*Ratio*	C-130	T.O.	*Ratio*
Ambient RH	29.3	35.8		66.2	65.5	
Nephelometer RH	15.7	11.8		36.8	23.4	
$\sigma_{sp,D<10\mu m}$, 550 nm	218.05	162.51	1.34	194.00	130.65	1.48
COV	*13.7%*	*15.8%*		*8.0%*	*9.9%*	
$\sigma_{ap,D<10\mu m}$, 550 nm	20.60	34.48	0.60	22.52	24.83	0.91
COV	*14.6%*	*72.9%*		*17.2%*	*33.0%*	

Intensive Parameters:	27-April-01, Leg #1			27-April-01, Leg #2		
	C-130	T.O.	*Diff*	C-130	T.O.	*Diff*
$f(RH)_{40-85\%}$	1.317	1.215	0.102	1.468	1.320	0.148
Std deviation	*0.041*	*0.047*		*0.055*	*0.022*	
ω, total aerosol	0.913	0.825	0.088	0.896	0.840	0.056
Std deviation	*0.007*	*0.092*		*0.014*	*0.043*	
FMF_{scat}	*0.572*	—		*0.550*	—	
Std deviation	*0.053*			*0.042*		

[a]As in Table 6, data are shown for those parameters measured on the Twin Otter, and FMF_{scat} is given in order to show that the aerosol was mixed for both of these legs.

nephelometers, whereas on the Ron Brown it was measured with a scanning-RH system employing TSI, Inc. nephelometers.

5.4. C-130 Versus Twin Otter

[75] A comparison of the set of parameters measured by both the Twin Otter and C-130, plus FMF_{scat} from the C-130, is shown in Table 7 for the two coordinated flight legs on 27 April – again omitting uncertainties because they were not determined for the Twin Otter. Here we do not adjust scattering for RH since all measurements were at low (<40%) RH, where f(RH) is nearly flat.

[76] The aerosol was a mix of fine and coarse mode particles ($FMF_{scat} \sim 0.5-0.6$) for both of these legs. Total light scattering was much higher on the C-130 (by ~35% and 50%), but $\sigma_{ap,D<10\mu m}$ was significantly lower, especially on the first leg. This is the case both on average and at the three times when the two platforms were in closest proximity. As a result $\omega_{D<10\mu m}$ is higher on the C-130 than on the Twin Otter, consistent with the direction of the discrepancies between the Ron Brown and Twin Otter (Table 6). The variability in scattering is similar on the two platforms, though again light absorption is much more variable on the Twin Otter.

[77] As with the Ron Brown/Twin Otter comparison, $f(RH)_{40-85\%}$ is lower on the Twin Otter, but here the discrepancies are much smaller. This may be because the C-130 and Twin Otter investigators used nearly identical approaches to measuring hygroscopic growth.

5.5. Ron Brown Versus Gosan

[78] Finally, there is one time period when the Ron Brown position and the winds were such that it is possible that Gosan measured the same air mass as had the Ron Brown 5.2 hours earlier, even though the platforms were separated by ~150 km (Figure 6 and Table 8). What we find is that while the two platforms measured nearly identical values of $\sigma_{sp,D<1\mu m}$, ~60% more supermicron scattering was measured at Gosan, yielding values of $\sigma_{sp,D<10\mu m}$ that were ~15% higher. This result is not consistent with chemical samples which give ratios of [soluble Ca]:[SO_4] and [Na]:[$NssSO_4$] that are ~1.2 and 1.6 times higher, respectively, on the ship than at Gosan.

[79] Because the fine mode aerosol is more light absorbing than the coarse mode aerosol, based only on the chemical data we would expect the ship to have lower $\omega_{D<10\mu m}$, which it does not. However, [BC]:[SO_4] is also ~60% higher at Gosan than on the ship, which *is* consistent with Gosan's lower values of $\omega_{D<1\mu m}$ (by 0.04) and $\omega_{D<10\mu m}$ (by 0.03). Thus it seems likely that the chemical composition of the fine mode aerosol differed at the two stations, despite the fact that submicron scattering agreed. In contrast, the [Na]:[soluble Ca] ratio at the two stations differ by only 15%, and the single scatter albedo of the ACE-Asia dust ($\omega \sim 0.96$; section 6) and sea salt ($\omega \sim 1.0$) are similar enough that different relative fractions of dust and sea salt could not explain the difference in $\omega_{D>1\mu m}$. However, caution should be used in over-interpreting the relationship between the chemical and optical measurements because the former were integrated over >7 hrs (R. Brown) and 24 hrs (Gosan) and may not reflect the aerosol composition during the 4 hr duration of the optical measurements.

[80] The Ångström exponents from the Ron Brown are higher than at Gosan, consistent with the ship's higher FMF_{scat}. Light scattering hygroscopic growth was higher at Gosan than on the Ron Brown, especially for the total aerosol. This is of particular interest since these two platforms both used TSI nephelometers and a scanning-RH system for measuring hygroscopic growth. In the other comparisons where large f(RH) discrepancies were observed the measurement techniques were different. Here, FMF_{scat} is higher on the Ron Brown and the discrepancy in the total aerosol $f(RH)_{40-85\%}$ is considerably greater than for the submicron aerosol, implying that the coarse mode aerosol at Gosan is more hygroscopic than at the Ron Brown. The chemical data from this comparison period indicate a higher ratio of sea salt to dust on the Ron Brown ([Na]:[soluble Ca] = 2.90) than at Gosan (2.52), which does not support this hypothesis. However, soluble Ca is a small and variable fraction of the total dust aerosol, so this difference (2.90 versus 2.52) may not be significant.

[81] Given the 4 hr sample period used at each station, it is not surprising that there were trends in concentration and aerosol type during the comparison period. On the Ron Brown, these trends were small (4% for $\sigma_{sp,D<10\mu m}$ and 12%

Table 8. As in Table 2, but for the Interplatform Comparison Between the Ron Brown and Gosan

	16-April-01		
Extensive Parameters:	R Brn	Gosan	*Ratio*
Ambient RH	73.4	79.8	—
Neph RH	61.5	41.1	—
$\sigma_{sp,D<10\mu m}$:	39.9	47.4	0.84
COV	*5.3%*	*10.8%*	
Precision uncert.	*1.5%*	*1.3%*	
$\sigma_{sp,D<1\mu m}$:	28.01	28.06	*1.00*
COV	*8.9%*	*13.2%*	
Precision uncert.	*1.7%*	*1.7%*	
Total/submicron			0.85
σ_{bsp}:	6.54	7.86	0.83
COV	*7.8%*	*9.0%*	
Precision uncert.	*6.1%*	*2.8%*	
$\sigma_{ap,D<10\mu m}$:	4.40	6.48	0.68
COV	*15.7%*	*6.6%*	
Precision uncert.	*6.9%*	*6.5%*	
$\sigma_{ap,D<1\mu m}$:	4.10	5.35	0.77
COV	*14.4%*	*12.7%*	
Precision uncert.	*7.4%*	*6.7%*	
Total/submicron			0.88

	16-April-01		
Intensive Parameters:	R Brn	Gosan	*Diff*
b:	0.164	0.166	−0.002
Std deviation	*0.008*	*0.006*	
Precision uncert.	*0.010*	*0.005*	
å:			
(450,700) mean	1.32	1.28	*0.040*
Std deviation	*0.09*	*0.09*	
Precision uncert.	*0.06*	*0.06*	
f(RH)$_{40-85\%}$:			
D < 10 μm *mean*	2.34	3.48	*−1.140*
Std deviation	*0.02*	*0.11*	
D < 1 μm *mean*	2.68	2.99	*−0.310*
Std deviation	*0.05*	*0.06*	
ω:			
D < 10 μm *mean*	0.907	0.879	*0.028*
Std deviation	*0.008*	*0.014*	
Precision uncert.	*0.006*	*0.007*	
D < 1 μm *mean*	0.875	0.838	*0.037*
Std deviation	*0.004*	*0.028*	
Precision uncert.	*0.008*	*0.008*	
D > 1 μm *mean*	0.966	0.945	*0.021*
Std deviation	*0.017*	*n/a*	
Precision uncert.	*0.034*	*0.026*	
FMF$_{scat}$:	0.712	0.587	*0.125*
Std deviation	*0.037*	*0.022*	
Precision uncert.	*0.016*	*0.013*	

for $\sigma_{sp,D<1\mu m}$), but at Gosan they were larger (19% for $\sigma_{sp,D<10\mu m}$ and 26% for $\sigma_{sp,D<1\mu m}$). Single scatter albedo also decreased very slightly (<0.01) on the Ron Brown and increased slightly (<0.02) at Gosan. However, these changes in all cases were nearly linear, so normalizing the data to the mid-point of the comparison leg does not change the results of the comparison.

5.6. Ensemble Comparison

[82] Direct interplatform comparisons should represent the best opportunity for testing whether similar measurements on different platforms yielded the same optical properties. Discrepancies during these comparisons are due to a combination of measurement (sampling and/or instrumental) imprecision and/or poor colocation of the two platforms. Discrepancies in the ensemble ("campaign-wide") comparison beyond those seen in the direct inter-platform comparisons can be attributed to real differences in the aerosol sampled by the platforms. This information is valuable in assessing whether the different platforms' data sets can be directly combined or should be considered complementary.

[83] In Table 9 we compare optical properties from the C-130 (for altitude <100 m), Gosan, and the Ron Brown for each platform's "full" data set (in the columns labeled "all data") as well as for subsets of the data, as described in section 3. The most directly comparable data sets should be "C-130: Yellow Sea and Gosan" *vs* "Gosan: winds 270°–330°" and "C-130: no Yellow Sea" *vs* "Ron Brown: all data." Within each of these categories averages and standard deviations are given for all of the data in that category as well as for three groupings of the data: "fine mode dominated" (FMF$_{scat}$ < 0.45), "mixed" (0.45 < FMF$_{scat}$ < 0.80), and "coarse mode dominated" (FMF$_{scat}$ > 0.80). Note that most of the direct interplatform comparisons fell into the "mixed" aerosol category.

[84] The three platforms compared here had fundamentally different sampling regimes (Table 1 and Figure 7). Because the sampling was not random or equivalent between platforms, we do not necessarily expect the concentration-dependent (extensive) properties to agree well amongst these "campaign-wide" data sets or to be regionally representative. In contrast, concentration differences do not affect the aerosol intensive properties, so these parameters present the most valid cases for the ensemble comparisons. Also, where all three platforms' aerosol intensive properties are in good agreement these data can be used to characterize the aerosol in this region during the ACE-Asia campaign.

[85] As such, we have calculated the means, ranges and the absolute uncertainties, as defined in section 4.5, for the aerosol intensive properties (Table 10). These data comprise our best estimates of the aerosol intensive optical properties for ACE-Asia. We also provide three measures of the parameters' uncertainty: 1) the nominal measurement uncertainty (95% confidence interval), which is based on laboratory studies of the instruments (see section 4.5); 2) the field precision, which is the RMS interplatform difference calculated from the suite of direct comparisons (Tables 2, 4, 6, 7, and 8); and 3) the interplatform range, as given by the minimum and maximum values in the three "all data" categories of the ensemble comparison (Table 9). Field precision is only calculated for the 0.45 < FMF$_{scat}$ < 0.80 category because there were fewer than three samples for the other two categories. We have not included the Twin Otter data in these estimates because these data (in particular single scatter albedo) appear to be outliers. We have also excluded the 04 April C-130/Ron Brown $\omega_{D<10\mu m}$ comparison because it, too, appears to be an outlier.

[86] Each of these types of "uncertainty" gives us a different set of information about the measurements. The nominal measurement uncertainties include both potential systematic biases and precision uncertainties, but they do not reflect differences that might arise from poor colocation of the platforms or from differences in aerosol sampling (inlet + plumbing) efficiencies. In contrast, the field precision and interplatform range include any instrument-to-instrument

Table 9. Results of the Ensemble Comparison Between the C-130, Gosan, and Ron Brown Campaign-Wide Data Sets for the Ambient and Measurement Relative Humidity and the Aerosol Extensive Properties, and the Aerosol Intensive Properties[a]

	C-130: All Data	C-130: No Yellow Sea	C-130: Yellow Sea and Gosan	Gosan: All Data	Gosan: Winds 270–330°	Ron Brown: All Data
Ambient RH	64.2 ± 15.2	60.1 ± 15.0	71.5 ± 12.7	74.5 ± 12.7	67.8 ± 16.4	73.4 ± 15.5
	58.4 ± 16.5	*53.2 ± 19.7*	*62.8 ± 11.4*	*68.2 ± 13.9*		*65.3 ± 10.7*
	66.3 ± 13.8	*62.0 ± 12.5*	*79.2 ± 8.4*	*73.7 ± 12.1*		*70.4 ± 14.9*
	65.8 ± 14.9	*58.5 ± 11.9*	*81.3 ± 6.1*	*84.1 ± 8.6*		*88.1 ± 7.9*
Measurement RH	28.7 ± 8.9	—	—	33.8 ± 7.6	—	54.5 ± 8.4
Extensive Parameters:						
$\sigma_{sp,D<10\mu m}$ 550 nm	130.5 ± 100.2	90.8 ± 42.5	203.5 ± 130.1	123.3 ± 82.1	156.4 ± 97.1	111.9 ± 75.7
	205.1 ± 140.6	*90.5 ± 35.3*	*303.5 ± 121.3*	*202.4 ± 66.2*		*197.16 ± 82.8*
	95.3 ± 40.8	*91.9 ± 44.0*	*105.3 ± 27.0*	*92.6 ± 46.5*		*88.82 ± 60.65*
	93.3 ± 44.8	*75.8 ± 43.8*	*124.0 ± 25.1*	*95.4 ± 53.0*		*142.35 ± 76.13*
$\sigma_{sp,D<1\mu m}$ 550 nm	53.7 ± 26.3	49.2 ± 26.9	62.4 ± 22.6	64.6 ± 34.2	60.1 ± 27.2	74.9 ± 52.2
	44.6 ± 20.7	*32.8 ± 15.3*	*54.8 ± 19.2*	*131.9 ± 83.4*		*78.0 ± 29.9*
	56.0 ± 25.8	*53.0 ± 26.8*	*64.9 ± 20.3*	*75.6 ± 43.2*		*57.5 ± 34.9*
	72.6 ± 34.7	*60.4 ± 33.8*	*98.2 ± 19.2*	*87.5 ± 49.0*		*122.1 ± 68.4*
$\sigma_{ap,D<10\mu m}$ 550 nm	13.4 ± 9.1	9.8 ± 5.5	20.2 ± 10.5	12.5 ± 8.1	18.1 ± 13.0	8.9 ± 4.7
	18.5 ± 12.7	*8.0 ± 4.2*	*27.6 ± 10.2*	*21.9 ± 11.3*		*14.3 ± 7.0*
	11.0 ± 5.4	*10.3 ± 5.8*	*13.2 ± 3.4*	*10.5 ± 5.3*		*7.6 ± 4.0*
	10.7 ± 4.5	*9.5 ± 4.8*	*13.3 ± 2.2*	*9.8 ± 6.0*		*10.3 ± 3.7*
$\sigma_{ap,D<1\mu m}$ 550 nm	14.2 ± 9.7	9.7 ± 5.5	22.1 ± 10.4	9.8 ± 6.0	13.2 ± 8.7	7.8 ± 3.8
	18.6 ± 12.7	*8.0 ± 4.2*	*27.6 ± 10.2*	*18.4 ± 10.3*		*10.1 ± 5.0*
	11.2 ± 5.7	*10.2 ± 5.9*	*14.4 ± 3.6*	*9.7 ± 5.0*		*6.8 ± 3.3*
	13.0 ± 2.9	*12.2 ± 3.3*	*14.2 ± 1.4*	*9.4 ± 5.7*		*9.7 ± 3.5*
Intensive Parameters:						
b 550 nm	0.102 ± 0.016	0.101 ± 0.016	0.105 ± 0.015	0.125 ± 0.021	—[b]	0.112 ± 0.014
	0.110 ± 0.016	*0.108 ± 0.016*	*0.115 ± 0.015*	*0.130 ± 0.011*		*0.115 ± 0.010*
	0.099 ± 0.015	*0.099 ± 0.015*	*0.097 ± 0.013*	*0.128 ± 0.021*		*0.114 ± 0.013*
	0.096 ± 0.019	*0.097 ± 0.019*	*0.083 ± 0.008*	*0.115 ± 0.019*		*0.106 ± 0.014*
å (450:700)	1.14 ± 0.47	1.25 ± 0.36	0.95 ± 0.58	1.39 ± 0.52	1.06 ± 0.55	1.35 ± 0.38
	0.56 ± 0.31	*0.57 ± 0.36*	*0.41 ± 0.28*	*0.75 ± 0.24*		*0.61 ± 0.25*
	1.38 ± 0.20	*1.40 ± 0.19*	*1.45 ± 0.16*	*1.55 ± 0.29*		*1.30 ± 0.24*
	1.68 ± 0.07	*1.62 ± 0.12*	*1.71 ± 0.07*	*1.90 ± 0.27*		*1.76 ± 0.13*
f(RH)$_{40-85\%}$: D < 10 μm	1.78 ± 0.28	1.84 ± 0.22	1.62 ± 0.31	2.27 ± 0.55	2.20 ± 0.41	2.37 ± 0.32
	1.53 ± 0.26	*1.68 ± 0.17*	*1.36 ± 0.21*	*2.06 ± 0.40*		*1.68 ± 0.34*
	1.87 ± 0.23	*1.88 ± 0.23*	*1.81 ± 0.23*	*2.28 ± 0.55*		*2.36 ± 0.21*
	1.87 ± 0.11	*1.85 ± 0.08*	*1.89 ± 0.16*	*2.51 ± 0.59*		*2.61 ± 0.23*
D < 1 μm	1.97 ± 0.23	2.00 ± 0.23	1.89 ± 0.21	2.36 ± 0.50	2.30 ± 0.38	2.68 ± 0.25
				2.18 ± 0.23		*2.26 ± 0.40*
				2.30 ± 0.40		*2.71 ± 0.21*
				2.77 ± 0.76		*2.74 ± 0.19*
ω: D < 10 μm	0.900 ± 0.025	0.900 ± 0.025	0.900 ± 0.024	0.894 ± 0.034	0.895 ± 0.021	0.898 ± 0.033
	0.912 ± 0.020	*0.913 ± 0.008*	*0.912 ± 0.025*	*0.904 ± 0.021*		*0.922 ± 0.024*
	0.895 ± 0.025	*0.898 ± 0.026*	*0.887 ± 0.018*	*0.888 ± 0.033*		*0.895 ± 0.028*
	0.886 ± 0.021	*0.880 ± 0.022*	*0.902 ± 0.010*	*0.888 ± 0.040*		*0.897 ± 0.044*
D < 1 μm	0.836 ± 0.050	0.854 ± 0.033	0.802 ± 0.057	0.853 ± 0.044	0.825 ± 0.045	0.866 ± 0.041
	0.796 ± 0.048	*0.835 ± 0.012*	*0.765 ± 0.043*	*0.819 ± 0.044*		*0.855 ± 0.046*
	0.854 ± 0.036	*0.858 ± 0.036*	*0.838 ± 0.032*	*0.856 ± 0.038*		*0.859 ± 0.034*
	0.889 ± 0.011	*0.886 ± 0.012*	*0.893 ± 0.006*	*0.876 ± 0.042*		*0.889 ± 0.047*
D > 1 μm	0.949 ± 0.027	0.935 ± 0.045	0.953 ± 0.016	0.938 ± 0.034	0.951 ± 0.020	0.951 ± 0.040
	0.955 ± 0.014	*0.957 ± 0.020*	*0.955 ± 0.013*	*0.953 ± 0.015*		*0.963 ± 0.014*
	0.931 ± 0.046	*0.931 ± 0.047*	*0.927 ± 0.035*	*0.923 ± 0.038*		*0.955 ± 0.025*
	0.868 ± 0.022	*0.860 ± 0.027*	*0.874 ± 0.018*	*0.867 ± 0.047*		*0.927 ± 0.071*
FMF$_{scat}$	0.530 ± 0.201	0.574 ± 0.162	0.450 ± 0.246	0.634 ± 0.169	0.470 ± 0.201	0.681 ± 0.148
	0.284 ± 0.119	*0.353 ± 0.085*	*0.218 ± 0.096*	*0.336 ± 0.064*		*0.389 ± 0.037*
	0.616 ± 0.095	*0.612 ± 0.095*	*0.641 ± 0.087*	*0.642 ± 0.091*		*0.658 ± 0.085*
	0.839 ± 0.036	*0.840 ± 0.037*	*0.833 ± 0.024*	*0.862 ± 0.053*		*0.862 ± 0.052*

[a]Given are means and standard deviations for (from top to bottom) the full data set in that category, then only for the data where FMF$_{scat}$ < 0.45, 0.45 < FMF$_{scat}$ < 0.80, and FMF$_{scat}$ > 0.80. Where only one value is shown, it is for the full data set.

[b]The hemispheric backscatter data from this period are known to be in error and so have not been included.

Table 10. Mean Values of the Aerosol Intensive Properties From the Three "All Data" Categories in Table 9; the Nominal Measurement Uncertainties of the Mean; the Average Discrepancy in That Parameter for the Direct Interplatform Comparisons; and the Interplatform Range of the Values From the Three "All Data" Categories in the Ensemble Comparison (Table 9)[a]

	Aerosol Type	Mean	Nominal Measurement Uncertainty	Field Precision (Direct)	Interplatform Range (Ensemble)
b 550 nm	$FMF_{scat} \leq 0.45$	0.118	0.030	– 0.021 –	0.020
	$0.45 < FMF_{scat} < 0.80$	0.114	0.017		0.029
	$FMF_{scat} \geq 0.80$	0.106	0.013		0.019
å (450:700)	$FMF_{scat} \leq 0.45$	0.64	0.78	– 0.13 –	0.25
	$0.45 < FMF_{scat} < 0.80$	1.41	0.48		
	$FMF_{scat} \geq 0.80$	1.78	0.35		
f(RH)$_{40-85\%}$	$FMF_{scat} \leq 0.45$	1.76	n/a	– 0.58 –	0.53
	$0.45 < FMF_{scat} < 0.80$	2.17			0.49
	$FMF_{scat} \geq 0.80$	2.33			0.40
ω:	$FMF_{scat} \leq 0.45$	0.913	0.026	– 0.016 –	0.018
D < 10 μm	$0.45 < FMF_{scat} < 0.80$	0.893	0.026		0.007
	$FMF_{scat} \geq 0.80$	0.890	0.022		0.011
D < 1μm	$FMF_{scat} \geq 0.80$	0.885	0.023	–	0.013
D >1 μm	$FMF_{scat} \leq 0.45$	0.957	0.031	–	0.010
FMF$_{scat}$	all data	0.629	0.092	0.072[b]	0.231

[a]Measurement uncertainty was not determined for f(RH), so it is not included here.
[b]Note that 8 of the 11 cases included here were for $0.45 < FMF_{scat} < 0.80$; two for $FMF \leq 0.45$; and one for $FMF \geq 0.80$.

differences (i.e. precision uncertainty), differences in sampling efficiencies, and differences due to poor colocation of the disparate platforms, but they do not include potential systematic bias in the in situ method. The data used to calculate the field precision is only from times when we attempted to colocate the two platforms whereas the interplatform range is based on data sets from different times and locations, so we would expect the latter range to be higher, given a large enough number of samples. The latter thus represents the most conservative estimate of that property's uncertainty for the ACE-Asia aerosol.

[87] For the Ångström exponent and single scatter albedo ($\omega_{D<1\mu m}$, $\omega_{D<1\mu m}$, and $\omega_{D>1\mu m}$), the nominal measurement uncertainties are greater than either the field precision or the interplatform range, which indicates that the primary concern is the absolute accuracy of the in situ measurements of these properties and not their repeatability. However, measured ranges exceed measurement uncertainties for FMF_{scat} and for the hemispheric backscatter fraction, when the aerosol is mixed or fine mode dominated. As we will discuss below, the interplatform discrepancies in FMF_{scat} can be attributed at least in part to understood differences in inlet systems and to different geographic sampling regimes. However, the observed discrepancies in b are not well understood. Finally, while the measurement uncertainty has not been determined for light scattering hygroscopic growth it is safe to say that the interplatform discrepancies for this parameter are also outside of the expected or acceptable range.

6. Discussion of Direct and Ensemble Comparison Results

[88] The direct interplatform comparisons and the ensemble comparison yield very similar results, particularly when the ensemble data are grouped so that geographically similar sampling regimes are compared. This is because the aerosol was much more dust-dominated in the Yellow Sea area than in the rest of the ACE-Asia study region (Table 9, FMF_{scat}). Thus the best ensemble comparisons will be between data sampled in similar regions and between groupings of data that are segregated by FMF_{scat}.

[89] The consistency in the interplatform and ensemble comparisons results lead us to believe that the observed discrepancies reflect systematic, methodological differences among the platforms. In this sense, the discrepancies serve as robust bounds on field-measurement uncertainties, which include both instrumental and sampling aspects. Looking at these comparisons we can conclude several things about the measurements:

[90] 1. The C-130 measured significantly more coarse mode and somewhat more fine mode aerosol than did the other three platforms. We expect the C-130 to sample relatively more coarse mode aerosol due to inlet differences (section 4.4), but all three platforms are expected to have sampling efficiencies ~1.0 for D < 1 μm aerosol. So while about a 10% enhancement to coarse mode scattering is predicted for the C-130 due to the combined effects of LTI enhancements and plumbing losses [*Anderson et al.*, 2003], the efficiencies for D < 1 μm aerosol should be 1.0. Thus we would expect only a ~5% positive bias in the total aerosol scattering for a mixed aerosol, such as was sampled for most of these comparisons, and no bias in the D < 1 μm scattering.

[91] In the ensemble comparisons, discrepancies in FMF_{scat} are indeed largest when the aerosol is coarse mode dominated, but FMF_{scat} is higher on the C-130 even when the aerosol is fine mode dominated. Also note (Table 9) that $\sigma_{sp,D<1\mu m}$ was highest on the C-130 and lowest on the Ron Brown. This is consistent with the fact that the D = 1 μm cut was made at the highest RH on the ship and the lowest RH on the C-130 (section 4.1).

[92] In the direct interplatform C-130/Gosan and C-130/ Ron Brown comparisons, the C-130 total scattering was on average 16% higher than the surface platforms (range: −3% to +38%), and C-130 scattering was 34% and 48% higher than on the Twin Otter for the two comparisons. Further, even for the D < 1 μm aerosol, scattering was on average ~5% higher on the C-130 than on the surface platforms. Similarly, in side-by-side comparisons between the C-130

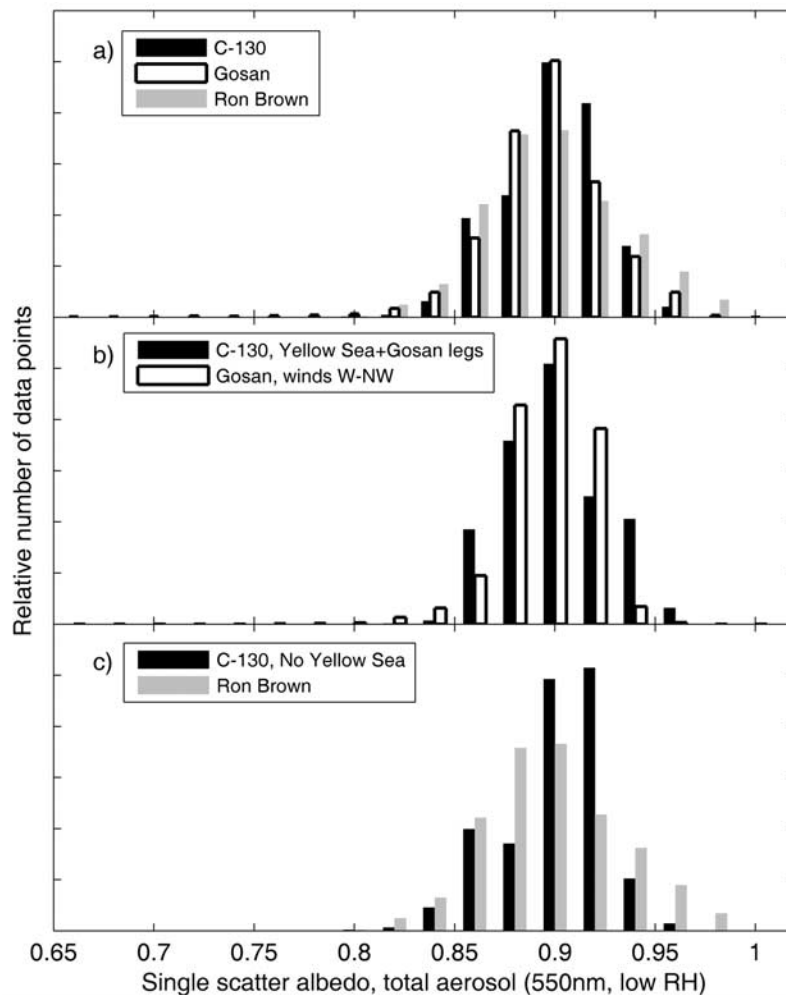**Figure 9.** As in Figure 8, but for $\omega_{D<10\mu m}$.

and the NASA P3-B flown for TRACE-P, *Moore et al.* [2004] found that the C-130 values of $\sigma_{sp,D<10\mu m}$ were 10%–25% higher for cases with FMF_{scat} ranging from 0.56–0.75. Values of $\sigma_{sp,D<1\mu m}$ were not compared. The P3-B had a solid diffuser inlet, which in side-by-side comparisons with the LTI showed differences of 20% for dry aerosol mass in the 3.5–5 μm diameter range [*Huebert et al.*, 2004]. Robust comparisons were not made for larger sizes.

[93] These collective results indicate that a) either the coarse mode enhancements on the C-130 are larger than expected and/or the coarse mode losses on the other platforms are larger than expected; b) the sampling efficiency of the D < 1 μm aerosol was not 1.0 on all four platforms; and/or c) the differences in the relative humidity at which the D = 1 μm cut was made produced the noted discrepancies in $\sigma_{sp,D<1\mu m}$.

[94] 2. Single scatter albedo generally agreed well across all platforms other than the Twin Otter. In the direct interplatform comparisons, discrepancies were <0.015 for all C-130/Gosan comparisons and ≤0.017 for all but two of the C-130/Ron Brown comparisons (Tables 2 and 4). However, ω was 0.03–0.09 lower on the Twin Otter than on the C-130 or Ron Brown. Single scatter albedo was also

0.02–0.04 higher on the Ron Brown than at Gosan during the one comparison available, but the two platforms were 150 km apart so we are less certain they were measuring the same air mass. Excellent agreement in ω (usually within 0.002) was also seen in the C-130 side-by-side comparisons with the NASA P3-B participating in TRACE-P [*Moore et al.*, 2004].

[95] Single scatter albedo also shows excellent agreement in the ensemble comparison of the C-130, Gosan and Ron Brown, with interplatform differences that are less than the measurement uncertainty (Table 10 and Figures 9–12). The good agreement we see in $\omega_{D>1\mu m}$ across the different platforms indicates that the relatively more efficient sampling of the coarse mode aerosol on the C-130 did not bias the D > 1 μm single scatter albedo measurements.

[96] 3. Hemispheric backscatter fraction, b, was 5–25% lower on the C-130 than at Gosan or on the Ron Brown. In both the direct and ensemble comparisons, hemispheric backscatter fraction is lowest for the C-130 and highest for Gosan for all FMF_{scat} categories. In the ensemble comparison, interplatform differences exceed the measurement uncertainty (Table 10). According to Mie calculations, b is generally higher for fine-mode than for coarse-mode aerosol, so lower b on the C-130 is consistent with its lower
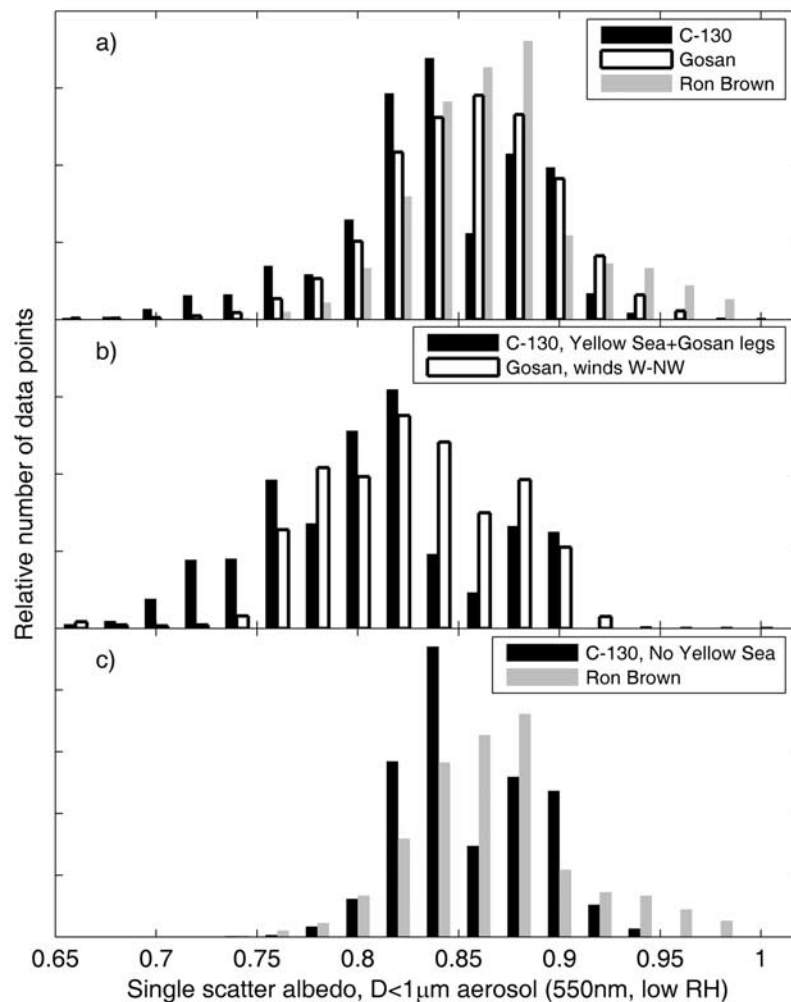
Figure 10. As in Figure 8, but for $\omega_{D<1\mu m}$.

values of FMF_{scat} and å. When a bimodal distribution is present higher values of b could be due to differences in the relative fractions of the fine-versus-coarse modes and/or differences in the mean diameter of the fine mode aerosol. However, on all three platforms b was *higher* for the coarse mode dominated cases than for the fine mode dominated cases (by $\sim 0.01-0.03$) indicating the opposite relationship between size and b than is given by Mie calculations and by the interplatform differences. This implies that either a) the relationship between aerosol size and/or shape and b is ambiguous for the ACE-Asia aerosol or b) we have over-estimated the precision of our measurements of b.

[97] One factor that may be confounding the expected relationship between aerosol size and the hemispheric backscatter fraction is particle shape. Unfortunately, the dependence of b on particle shape is not well understood, though it is possible that shape effects produce the observed inverse relationship between FMF_{scat} and b. Of import is that the optical measurements were made at low RH and that the primary coarse mode component for the data presented here was dust, which is both nonspherical and not very hygroscopic. If shape effects have caused FMF_{scat} and b to be inversely related, this result stands in opposition to the modeling study by *Kalashnikova and Sokolik* [2002]

which asserts that b is *lower* for sharp-edged aerosol than for spherical aerosol of the same geometric diameter. It also does not explain why the C-130, which measured relatively more coarse mode aerosol than the other platforms, had higher values of b. One possibility is that we are under-correcting for the truncation of the forward-scattered signal (i.e., $0°-7°$ scattering) in the total scattering measurement. Because there is relatively more forward scatter for the larger aerosol, this would bias b high for the coarse aerosol.

[98] 4. There are large discrepancies in light scattering hygroscopic growth, with $f(RH)_{40-85\%}$ systematically higher on the surface-based platforms (Ron Brown, Gosan) than on the aircraft (C-130, Twin Otter). In the direct comparisons, the Gosan and Ron Brown $f(RH)_{40-85\%}$ values were, respectively, on average a factor of 1.42 and 1.25 higher than on the C-130. In turn, $f(RH)_{40-85\%}$ on the C-130 was a factor of 1.10 higher than on the Twin Otter, and on the Ron Brown it was a factor of ~ 1.50 higher than on the Twin Otter. These large discrepancies are similarly present in the ensemble comparison (Table 9 and Figure 13), with one exception: the "C-130: No Yellow Sea" and "Ron Brown: all data" values for the D < 10 μm aerosol are in excellent agreement. Also, the C-130 and Gosan data are consistent in showing that f(RH) is lower in the Yellow Sea
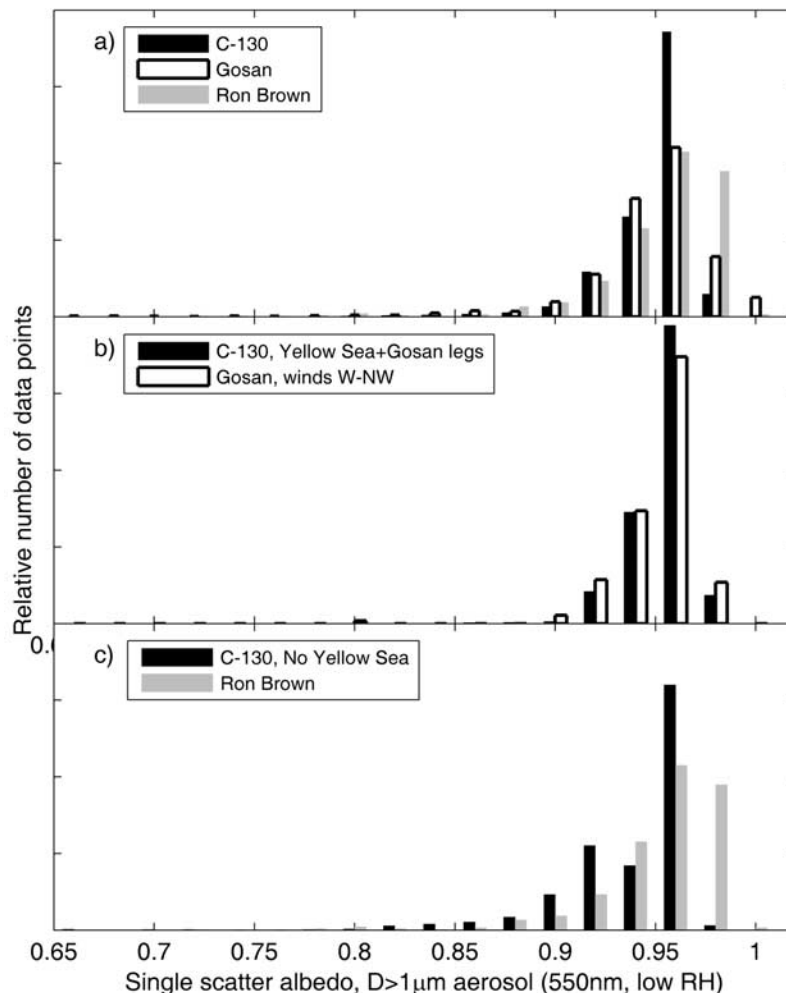
Figure 11. As in Figure 8, but for $\omega_{D>1\mu m}$.

region than in the rest of the ACE-Asia study region. In all cases the aerosol becomes more hygroscopic as FMF_{scat} increases, consistent with a coarse mode dominated by dust (Table 9), though the correlation between FMF_{scat} and $f(RH)_{40,85}$ is much more robust on the C-130 and Ron Brown than at Gosan. We also note that at times the Gosan values appear unrealistically high for the size and type of aerosol that were present during ACE-Asia (Figure 14). Despite these general consistencies the discrepancies in $f(RH)_{40-85\%}$ – particularly between the C-130 and Gosan – are large for both the total aerosol and the submicron aerosol.

[99] The relatively larger differences in $f(RH)_{40-85\%}$ for the surface-vs-aircraft comparisons lead to the conclusion that the scanning-RH system employing TSI, Inc. nephelometers and the two-point system using Radiance Research nephelometers give fundamentally different measurements of $f(RH)$. Here we consider several potential sources of error in the $f(RH)$ data, though we do not believe any are sufficient to explain the observed discrepancies. First, on the C-130 two different nephelometers were used to measure low- and high-RH scattering, so we checked for relative biases between them when the ambient air was dry enough that the high-RH nephelometer RH was <60%. At these

times, we adjusted the high-RH scattering to the low-RH nephelometer relative humidity using a best-guess value for γ (equation (6)). During these times, $\sigma_{sp,RRwet} = 1.01 * \sigma_{sp,RRdry} + 1.3$ Mm^{-1}. This 1% difference is not only very small but would, if anything, produce a high bias in the C-130 $f(RH)_{40-85\%}$ values.

[100] Second, the dried aerosol needs time to hydrate fully, so we confirmed that all of the humidifier systems had similar residence times.

[101] Third, we have considered the fact that the angular measurement range of the Radiance Research nephleometers is unknown, and that there could be significant differences in the angular correction factor for hydrated versus dry aerosol. Such a difference would not be accounted for here. However, the Ron Brown $f(RH)$ measurements (not shown) indicate that the aerosol Ångström exponent is nearly invariant with changes in RH (except for volcanic aerosol), implying that there should not be large differences in the angular truncation correction factors for the dry versus hydrated aerosol. Thus this source of error is unlikely to be large, unless the angular measurement range of the two instruments is different.

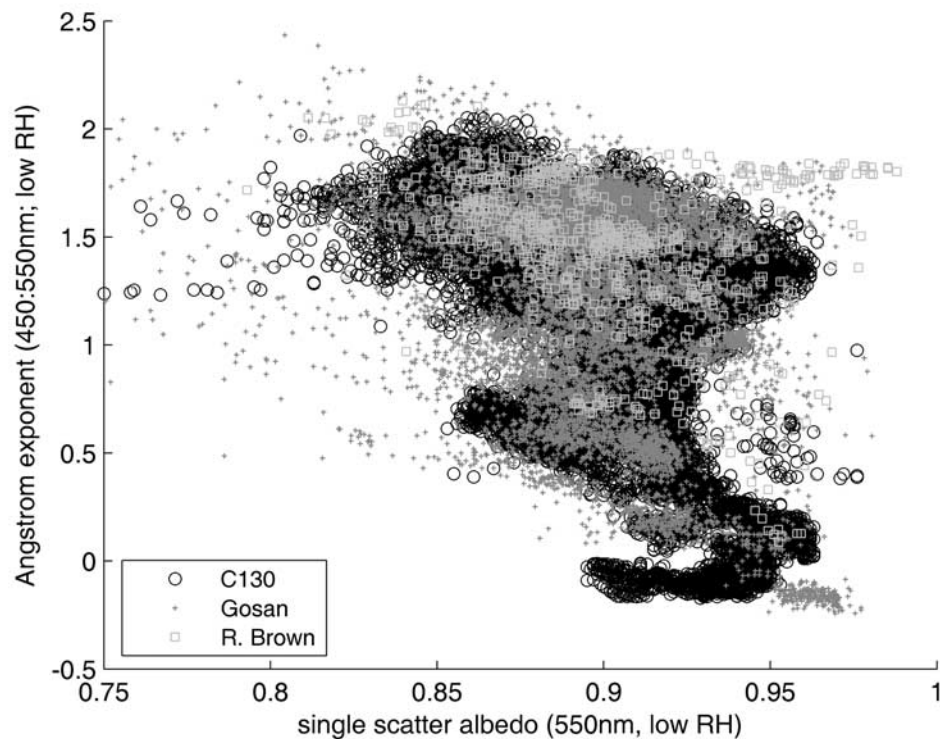[102] Fourth, the wavelength range over which the Radiance Research nephelometers measure σ_{sp} is not well

Figure 12. The size-dependence of $\omega_{D<10\mu m}$ was similar on all three platforms, as is seen when it is plotted against the Ångström exponent.

known, and preliminary tests indicate their peak response varies from instrument to instrument (N. Ahlquist, personal communication). On the C-130, both Radiance nephelometers were modified for a peak sensitivity of 540 nm [*Anderson et al.*, 2003], but the exact wavelength of the Twin Otter f(RH) data is not known. According to the Ron Brown multi-wavelength f(RH) data, f(RH) decreased along with wavelength such that the C-130 540 nm f(RH) values should be slightly (<0.10) lower than the Gosan and Ron Brown 550 nm f(RH), but not as much lower as was observed.

[103] Fifth, in all systems it is possible that particle losses are biasing the f(RH) values low. For the scanning RH systems (Gosan; Ron Brown) these losses translate
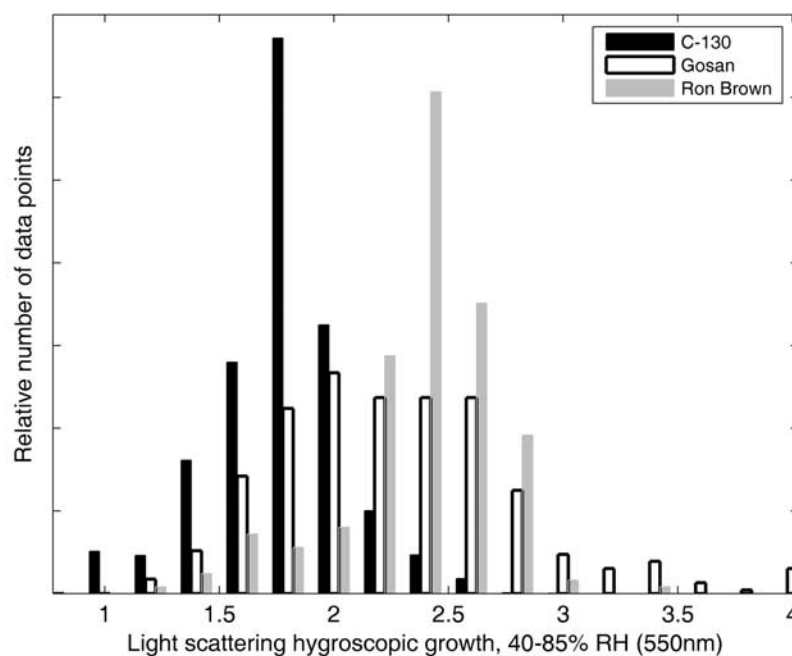
Figure 13. As in Figure 8a, but for f(RH)$_{40-85\%}$. Here we only show each platform's full data set, as there are not enough measurements available for a meaningful comparison of the subsets of data.
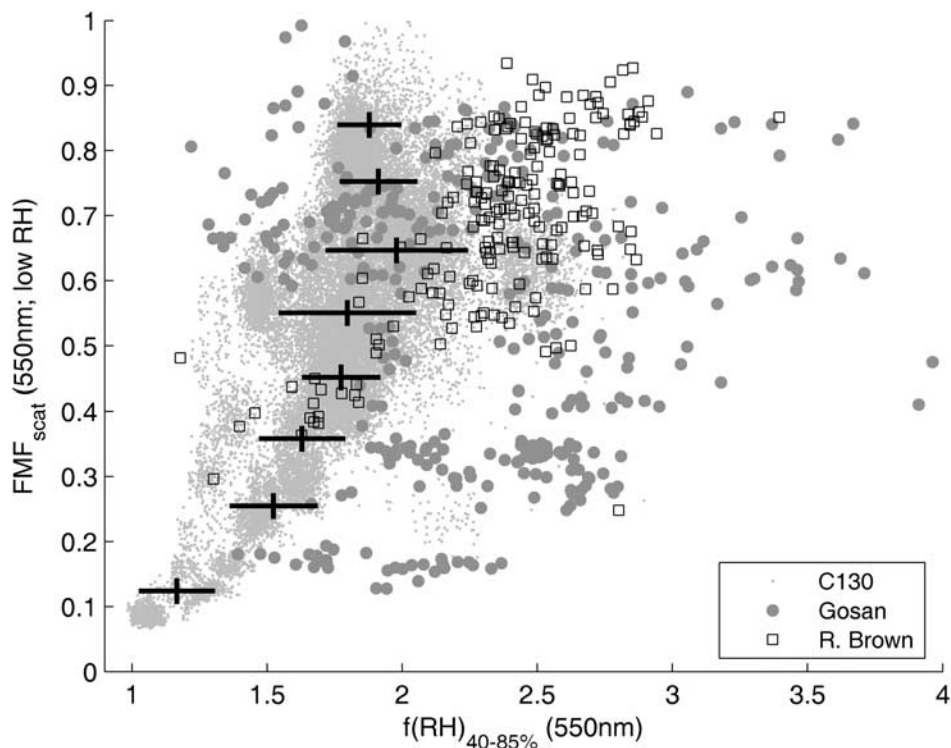
Figure 14. Variations in light scattering hygroscopic growth, $f(RH)_{40-85\%}$, with aerosol size reflect changes in composition with size. Here we compare the relationship between the two for data from the C-130 (gray small dots), Gosan (large gray dots) and the Ron Brown (open squares). Also shown is the mean and standard deviation of $f(RH)$ within bins of FMF_{scat} for the C-130 data only.

into errors only if the aerosol losses are size or relative humidity dependent. The two point system (C-130; Twin Otter) is more sensitive to this because the error depends on the total aerosol loss and not just size-dependent aerosol loss. Tests of the Gosan and Ron Brown systems show that at low RH there is about a 5% loss (decline in scattering) through the humidifer for D < 1 μm aerosol and ~5–15% for D < 10 μm aerosol. The Gosan and Ron Brown data have been adjusted to correct for these losses [*Sheridan et al.*, 2001; *Carrico et al.*, 2003]. On the C-130 and Twin Otter, potential losses in the humidification system are not expected to be significant, but tests are needed to confirm this.

[104] Finally, there is the question of whether the relative humidity values we are using to calculate $f(RH)$ both are accurate and reflect the RH in the optical sample volume. For all systems, RH sensors were compared to each other and significant biases were not seen. For the scanning-RH systems, relative humidity was measured inside the TSI, Inc. nephelometer sample volumes. However, for the two-point systems the high-RH nephelometer relative humidity was measured at the inlet and outlet of the nephelometers, and the average of these two measurements was used. On the C-130, the RH measured at the outlet was on average 2.0 ± 4.3% higher than at the inlet. Unless the aerosol is somehow warmed and then nearly equally cooled between the inlet and the outlet an RH error estimate of 3% is therefore quite conservative, given that there did not appear to be a bias between the two sensors. Depending on the aerosol hygoscopicity, this would produce a bias in

$f(RH)_{40-84\%}$ of between ~5% ($\gamma = 0.325$) and ~20% ($\gamma = 0.825$), which would account for some, but not all, of the observed large discrepancies in $f(RH)_{40-85\%}$. Radial gradients in RH within the sample volume could also be confounding the results.

[105] Finally, there is the question of how well the two-point gamma fit method describes the overall aerosol hygroscopic growth behavior. We tested for this by calculating $f(RH)_{40-85\%}$ using both the two-point gamma-fit method and the more complex curve-fitting method, applying both to the Ron Brown hygroscopic growth data sets. Because in this test the two-point method is anchored at 40% and 85% RH, the two data sets agree for $f(RH)_{40-85\%}$. However, the two-point method will tend to over-estimate aerosol hygroscopic growth at "intermediate" values of RH (i.e. for adjustments to 60% or 70% RH) because the curve shape is more shallow. This is most dramatically the case when the aerosol is deliquescent and the RH is still below the deliquescence point. This is important, because the ambient atmosphere RH in the boundary layer was often in the 40–70% range.

7. Summary of Aerosol Optical Properties

[106] The data in Tables 9 and 10 summarize the aerosol hemispheric backscatter fraction, Ångström exponent, hygroscopicity, and single scatter albedo as measured in situ in the boundary layer (<100 m altitude) during the ACE-Asia field campaign. Because the data are broken down by FMF_{scat}, we can separately bound these properties for the fine and coarse mode aerosol, which tend to be chemically

distinct. Confidence in these data are given by the magnitudes of their uncertainty, precision and range (Table 10).

[107] On all three platforms light scattering was, on average, roughly equally due to fine and coarse mode aerosol. Chemical data (not shown) indicate this was a mix of dust and pollution, with sea salt sometime also comprising part of the coarse mode on the Ron Brown. As expected for a dust coarse mode, light scattering hygroscopic growth is lower when the aerosol is coarse mode dominated. However, even when FMF_{scat} is low light scattering increases by $\sim 6\%-44\%$ when adjusted to the ambient RH of $\sim 55-70\%$ (Table 9 and equation (5)). When the aerosol is fine mode dominated, scattering increases by $13\%-65\%$. This mixed aerosol state has implications for satellite retrievals (which measure full-column properties) and is informative for chemical transport models simulating aerosol field for this region and for radiative transfer models which convert dry aerosol loads to ambient-RH scattering.

[108] The most well-constrained parameter in Table 10 is the single scatter albedo, which has been separately measured for the fine and coarse mode aerosol. The single scatter albedo of pollution is most closely approximated by $\omega_{D<1\mu m}$ only when FMF_{scat} is high, giving a well-constrained mean of $0.876-0.889$. Similarly, ω for the coarse mode aerosol is given by the $D > 1\ \mu m$ data when FMF_{scat} is low, or $\omega = 0.953-0.963$. While on the C-130 the coarse mode aerosol was clearly dominated by dust [*Anderson et al.*, 2003], sea salt was a significant fraction of the coarse mode during some periods on the Ron Brown. *Quinn et al.* [2004] categorized the Ron Brown data by air mass type, based on source region using backtrajectories. For the earlier segment of the data included here (days 91.0–99.2) the coarse mode aerosol was, by mass, about equal amounts dust and sea salt, whereas from days 101.0–104.5 it was clearly dust-dominated. Coarse mode concentrations were considerably higher ($\sim 3-8$ times higher by mass) during the dust-dominated periods. Where there was a mix of dust and sea salt present, $\omega_{D>1\mu m}$ was 0.953 ± 0.045, whereas during the dust events it was 0.962 ± 0.016. The lower values for the mix may result from the fact that there was also relatively more pollution present at these times, and either the pollution could be attached to the dust/sea salt or the tail of the fine mode pollution could be influencing the $D > 1\ \mu m$ measurement. In any case, ω is not significantly different for these two periods.

[109] The high value of ω at 550 nm for dust agrees very well with other mineral dust measurements at mid-visible wavelengths, as well as with some recent modelling studies. In early studies of Asian dust, *Clarke and Charlson* [1985] found $\omega_{dust} = 0.97$ based on two years of size-resolved scattering and absorption measurements at Mauna Loa. *Clarke et al.* [1996] made the first measurements of Saharan dust ω and obtained values of $0.96-0.97$. Subsequently, using aircraft measurements of the Asian dust plume over the Pacific, *Clarke et al.* [2001] again found $\omega_{dust} = 0.97 \pm 0.01$. More recently, *Haywood et al.* [2003] found $\omega_{dust} = 0.97 \pm 0.02$, also using in situ (TSI nephelometer and PSAP) measurements of Saharan dust. *Kaufman et al.* [2001] retrieved $\omega_{dust} = 0.97$ over the Sahara via satellite measurements. In a modeling study applying discrete dipole approximation techniques, *Kalashnikova and Sokolik* [2002] got $\omega = 0.96-0.97$ for sharp-edged dust of a size

and composition determined from real samples of Asian atmospheric dust.

[110] The ensemble data (Table 9) also indicates that pollution is more light-absorbing in the Yellow Sea than in the rest of the ACE-Asia study region (i.e. $\omega_{D<1\mu m} = 0.854$ for "C-130: no Yellow Sea" versus 0.802 for "C-130: Yellow Sea and Gosan"; and $\omega_{D<1\mu m} = 0.853$ for "Gosan: all data" versus 0.825 for "Gosan: winds 270–330°"). There is also an indication that the supermicron aerosol is more light absorbing in this area, though the difference here is only $0.01-0.02$ and may be the result of the tail of the more light-absorbing fine mode aerosol influencing the $D > 1\ \mu m$ aerosol.

[111] More striking is the decrease in submicron ω with FMF_{scat} on all platforms. The C-130 data indicate a relationship between the two that roughly follows $\omega_{D<1\mu m} = 0.794 + 0.11 * FMF_{scat}$. *Clarke et al.* [2004] also make note of this relationship using measurements of particle size before and after thermal heating, which removes the volatile components of the aerosol. They attribute the change in ω and volatility of the submicron aerosol in the presence of dust to the preferential accumulation of sulphate and other species onto the dust, thereby leaving relatively more light-absorbing species in the fine mode. It is also possible that the source regions are different when the aerosol is fine mode dominated than when it is coarse mode dominated and that the fine mode aerosol is more light absorbing in the source regions associated with the low FMF_{scat} (i.e. dusty) events. In either case, the relationship between $\omega_{D<1\mu m}$ and FMF_{scat} appears to be robust.

8. Implications for Radiative Forcing

[112] In order for these data to be useful in radiative forcing calculations we must be confident that they reflect the true optical properties of the ambient atmospheric aerosol and that they do so over the range of altitudes where there is significant aerosol loading. Here we examine whether this is the case, then look at how uncertainties in the optical properties translate into uncertainties in radiative forcing.

[113] 1. How well do the optical properties derived from the in situ measurements describe the atmospheric aerosol under ambient conditions? We have noted that there may be sampling biases in the in situ measurements and that the light scattering and absorption measurements are made at low RH. To calculate ambient-RH scattering we rely on our empirically derived parameterization of scattering hygroscopic growth, which may be in error (as is reflected by the large interplatform discrepancies in f(RH)). More significant, no measure is made of how σ_{ap} changes with RH so we must assume that f(RH) = 1 for light absorption. This may introduce small errors in our in situ measurements of light extinction and optical depth and more significant errors in single scatter albedo.

[114] We can test for sampling biases, error in the RH-adjustments, and other systematic biases in our in situ measurements by comparing them to coincident remote sensing measurements, which are by definition made under ambient conditions. Both the C-130 and Twin Otter aircraft had sun photometers on board during ACE-Asia, and closure studies with the in situ data sets have been done
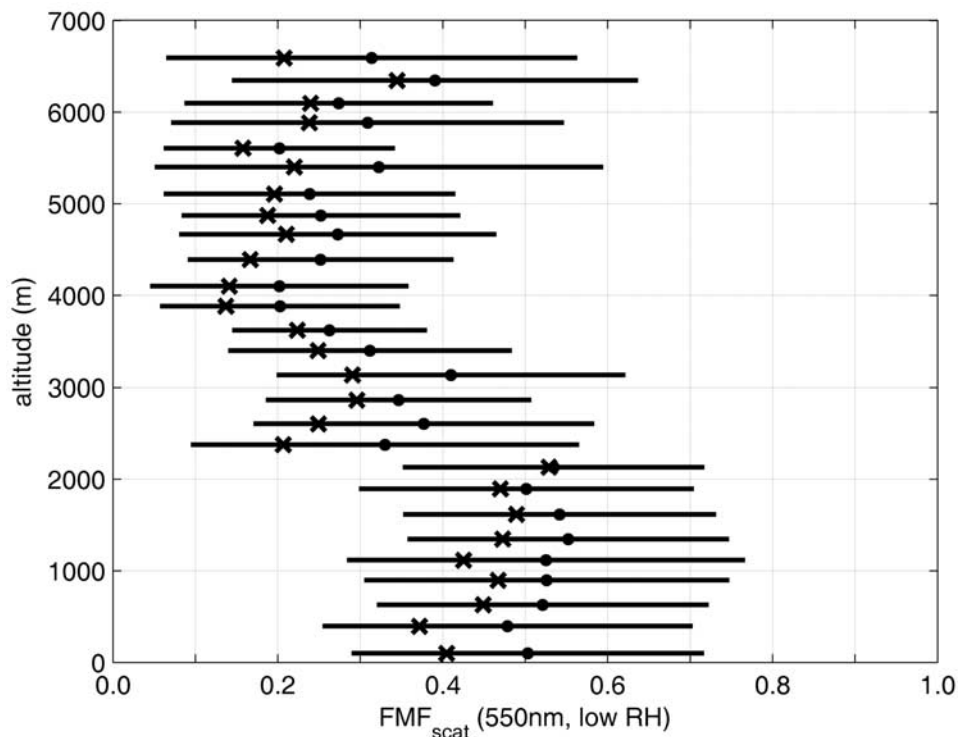
Figure 15. The mean (solid dots) and 1-sigma range of FMF_{scat}, averaged over 250 m altitude bins, is shown for the full C-130 data set. The extinction-weighted mean FMF_{scat} in each altitude bin is also shown (crosses). These values are somewhat lower because the high extinction events measured by the C-130 were usually associated with dust storms, even at low altitudes.

for 28 profiles on the C-130 [*Redemann et al.*, 2003] and 14 profiles on the Twin Otter [*Schmid et al.*, 2003]. The sun photometers used in these two studies are quite similar, the difference being that the Twin Otter photometer (AATS-14) has 14 wavelength channels and the C-130 photometer (AATS-6) has 6 wavelength channels. Both were deployed by the same research group at NASA-Ames Research Center, so data reduction procedures were similar for the two data sets.

[115] On the C-130, the comparison between the sunphotometer and in situ derived layer aerosol optical depths (AOD) at 550 nm showed agreement within the measurement uncertainties in 25 out of 28 profiles [*Redemann et al.*, 2003]. Light extinction was, on average, 6% higher for the in situ measurements and was well-correlated with the sun photometer values ($r^2 = 0.79$). These samples were roughly equally distributed between fine mode dominated, coarse mode dominated and mixed aerosol cases.

[116] Stratification of the data by ambient relative humidity reveals that at low RH (<20%) in situ light extinction was ∼15% lower than the sun photometer values and at high RH (>80%) they were ∼25% higher. This implies that, if anything, light scattering hygroscopic growth is overestimated by the in situ measurements. This is striking given that the C-130 f(RH) values are considerably lower than those on the Ron Brown and at Gosan, though as mentioned earlier the gamma-fit method used on the C-130 for f(RH) may over-estimate f(RH) at moderate RH. When stratified by FMF_{scat}, in situ extinction is ∼12–13% higher when the aerosol is mixed or coarse mode dominated. However, for

FMF_{scat} > 0.80, extinction is only 1% higher in the in situ data set. Recall that we expect about a 10% high bias in the C-130 in situ measurements of coarse mode light scattering, which is generally consistent with these closure study results.

[117] On the Twin Otter, the in situ 550 nm extinction was on average 13% lower than the sun photometer extinction and the correlation between the two data sets was somewhat lower than on the C-130 ($r^2 = 0.64$). A low bias in the Twin Otter in situ measurements is consistent with the results of the Twin Otter/Ron Brown and Twin Otter/C-130 interplatform comparisons presented in sections 5.3 and section 5.4, and these combined results point to there being inlet and/or plumbing losses on the Twin Otter. However, the extinction discrepancies in the closure study with the sun photometer are not clearly correlated with the relative abundance of coarse-vs-fine aerosol or with ambient RH.

[118] Unfortunately the sun photometer cannot separately measure scattering and absorption so we cannot test for errors in σ_{ap} via these radiative closure studies. This is important because σ_{ap} (and thus ω) is determined for low RH only, and ambient-RH absorption may differ from the dry value. The best test for absorption closure comes from comparisons with flux divergence, as measured using an aircraft-based radiometer. In this approach atmospheric forcing, which is due fully to light absorption, is given by the difference between the forcing at the top of the atmosphere and the forcing at the surface. Such radiometric measurements were made on board the C-130, but flux
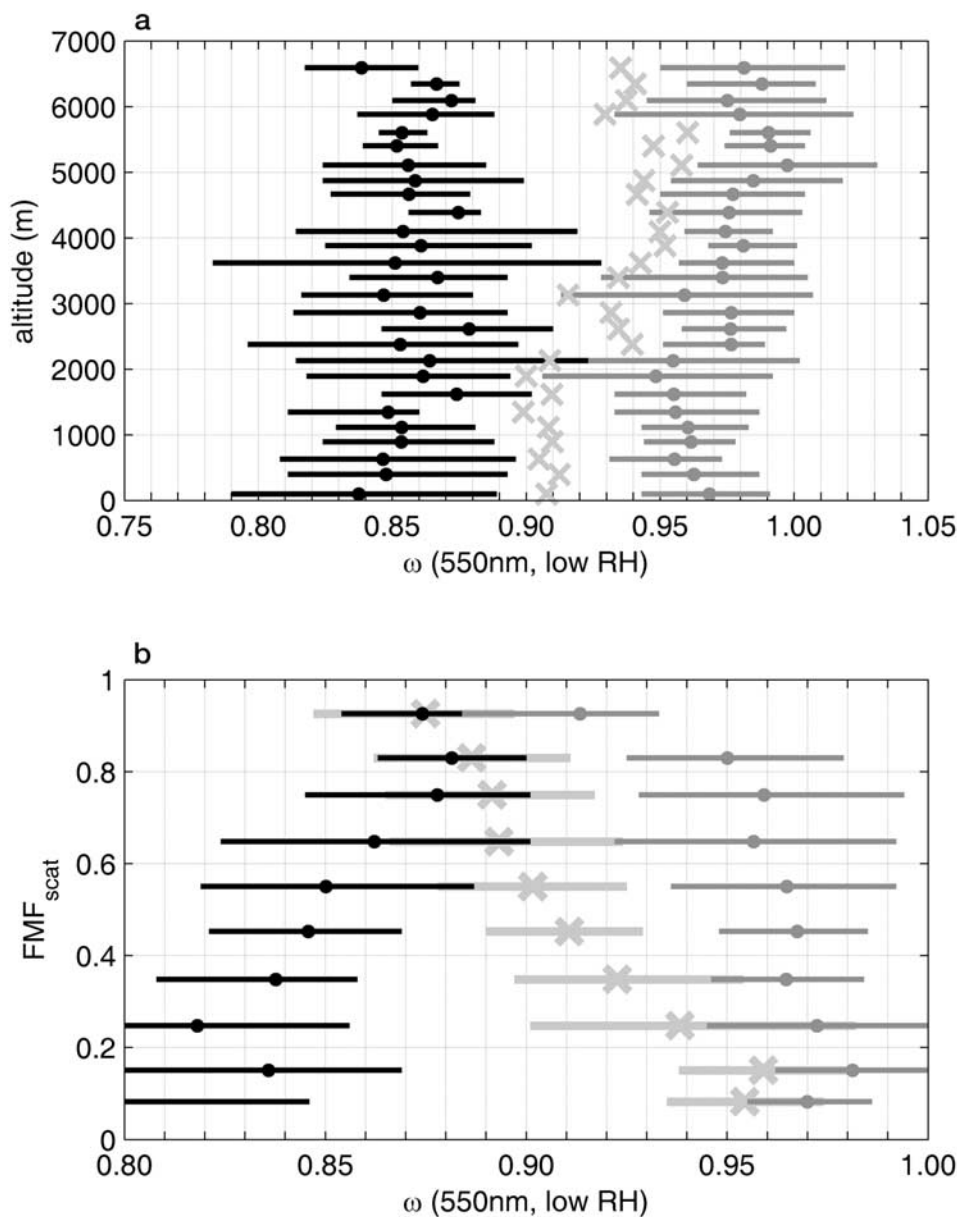
Figure 16. The mean and 1-sigma range of the single scatter albedo of the submicron aerosol ($\omega_{D<1\mu m}$; medium grey), the supermicron aerosol ($\omega_{D>1\mu m}$; black), and the total aerosol ($\omega_{D<10\mu m}$; light grey crosses) for the full C-130 data set are shown binned by (a) 250 m increments in altitude and (b) 0.1 increments of FMF_{scat}. Note that values $\omega > 1.0$ result when $\sigma_{ap} \sim 0.0$ so the measured value of σ_{ap} is dominated by instrumental noise, which can have negative values.

divergence has not yet been calculated so closure with in situ σ_{ap} will need to be the subject of a future study.

[119] 2. How well do the surface data represent what is going on in the full column? The values given in Tables 9 and 10 represent our best estimates of the ACE-Asia aerosol optical properties, but only for measurements near the surface (i.e., <100 m altitude). Because the C-130 aircraft sampled aerosol over a range of altitudes we can also examine how representative the surface data are of the full column. Key indicators are shown in Figures 15–18.

[120] We have noted that the dominant types of aerosol present in the study region were pollution and dust and that the near-surface scattering was, on average, due about

equally to these two aerosol types (FMF_{scat} in Table 9 and Figure 8). From the C-130 data we see that this was the case up to ~2.25 km altitude, but higher than this there is a shift in FMF_{scat} such that dust has a stronger influence on the aerosol optical properties (Figure 15). *Quinn et al.* [2004] similarly concluded that there was relatively more coarse mode aerosol aloft than at the surface using in situ and sun photometer data from the Ron Brown.

[121] The total aerosol single scatter albedo, $\omega_{D<10\mu m}$, also shifts at 2.25 km altitude, with higher values aloft (Figure 16). However, most of the change in $\omega_{D<10\mu m}$ can be attributed directly to the change in the relative fractions of dust and pollution, because the single scatter albedo of

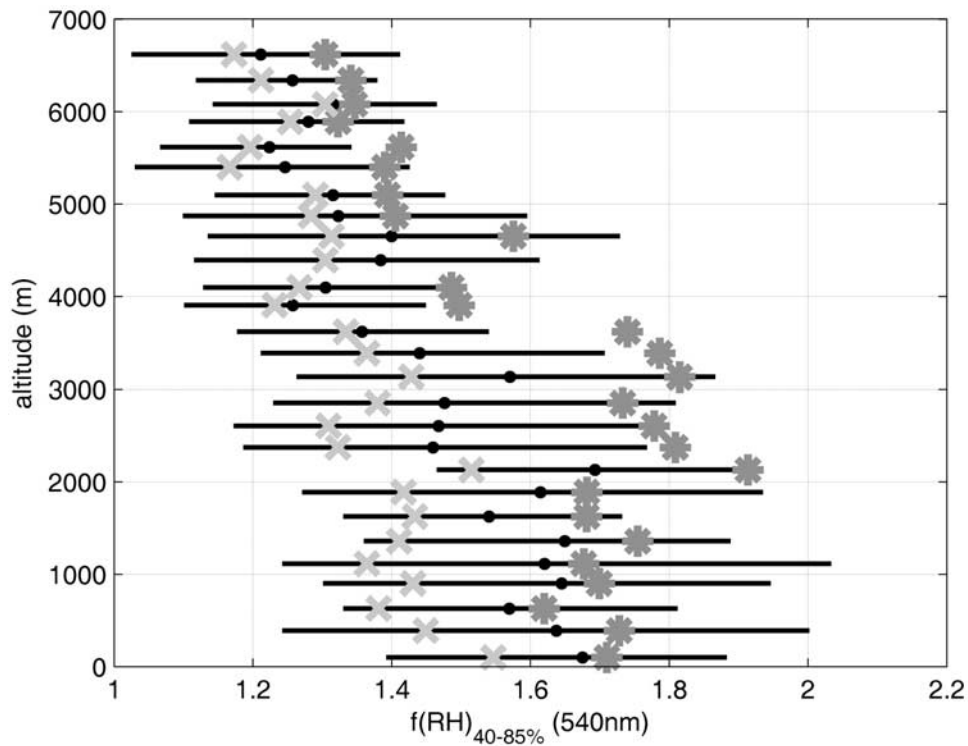**Figure 17.** Shown is the mean and 1-sigma range of the D > 10 μm aerosol light scattering hygroscopic growth, f(RH)$_{40-85\%}$, for all data (black), as well as the mean only of f(RH)$_{40-85\%}$ for those data where FMF$_{scat}$ ≤ 0.45 (light gray crosses) and those data where FMF$_{scat}$ ≥ 0.80 (medium gray asterisks).
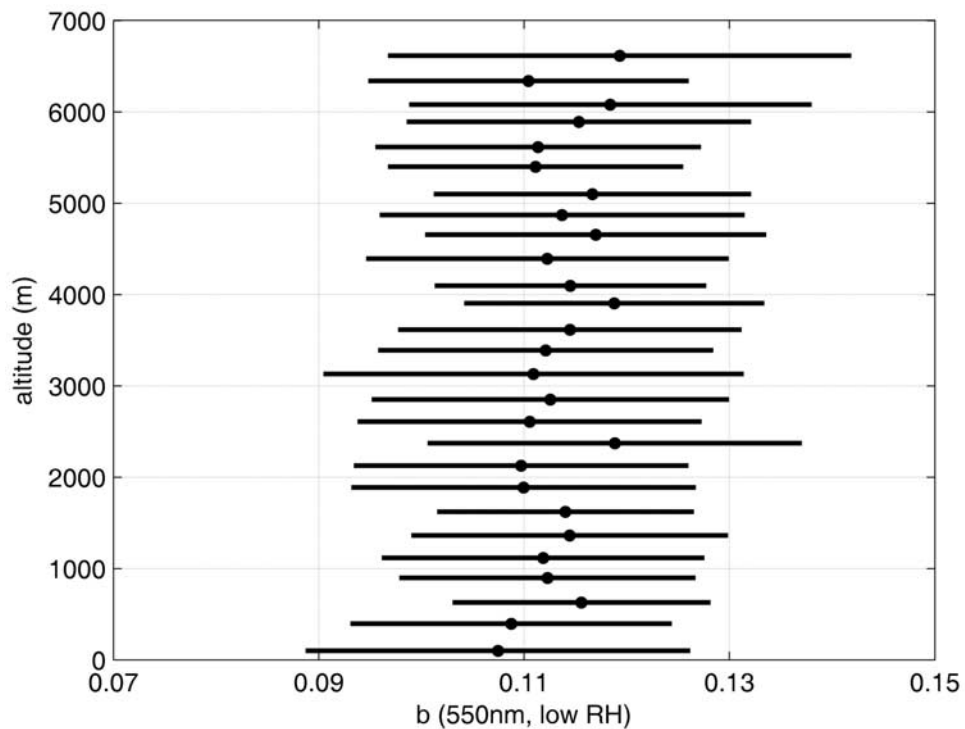

Figure 18. As in Figure 16a, but for the mean and 1-sigma range of the hemispheric backscatter fraction at low RH and 550 nm.

Table 11. Uncertainties in Single Scatter Albedo (ω) and Hemispheric Backscatter Fraction (b) Produce Uncertainties in the Clear-Sky, Top-of-the-Atmosphere Direct Aerosol Radiative Forcing per Unit Optical Depth ($\Delta F_{TOA}/\tau$), or Forcing Efficiency[a]

			$\Delta F_{TOA}/\tau$, W/m^2		Ratio	$\Delta F_{TOA}/\tau$, W/m^2		Ratio
			Min	Max	(Max/Min)	Min	Max	(Max/Min)
Aerosol Type by FMF$_{scat}$:	ω	b	$R_s = 0.07$ (Ocean):			$R_s = 0.15$ (Land):		
FMF$_{scat} \leq 0.45$	0.913	0.098−0.138	−68.4	−82.8	1.21	−50.9	−62.9	1.24
Mixed aerosol	0.893	0.085−0.143	−60.5	−81.3	1.34	−42.8	−60.2	1.41
FMF$_{scat} \geq 0.80$	0.890	0.087−0.125	−61.0	75.1	1.23	−43.0	54.7	1.27
FMF$_{scat} \leq 0.45$	0.887−0.939	0.118	−72.2	−79.7	1.10	−52.2	−62.2	1.19
Mixed aerosol	0.867−0.919	0.114	−68.0	−75.4	1.11	−47.2	−57.1	1.21
FMF$_{scat} \geq 0.80$	0.868−0.912	0.106	−65.3	−71.4	1.09	−45.0	−53.3	1.18
Mixed aerosol	0.867−0.919	0.085−0.143	−57.2	−85.3	1.49	−38.1	−65.4	1.72

[a]Values are at 550 nm (and thus do not include infrared effects) and are calculated for surface reflectances (R_s) representative of the ocean and land surfaces in the ACE-Asia study region.

pollution (approximated by $\omega_{D<1\mu m}$) is essentially invariant with height, and $\omega_{D>1\mu m}$ increases only slightly with altitude. Thus, models applying the values of $\omega_{D<1\mu m}$ and $\omega_{D>1\mu m}$ given in Table 10 should be accurate at calculating total aerosol single scatter albedo, as long as they also use an appropriate vertical structure for FMF$_{scat}$.

[122] Light scattering hygroscopic growth, f(RH)$_{40-85\%}$, of the total aerosol also decreases with altitude. However in this case we cannot attribute this solely to the decrease in FMF$_{scat}$ since both the submicron and supermicron aerosol also both become less hygroscopic with altitude. Thus the values of f(RH) for either the D < 1 μm or the total aerosol measured at the surface appear not to reflect the state of the lofted aerosol. In contrast, the aerosol hemispheric backscatter fraction is nearly invariant with altitude (Figure 18), which is surprising given that b is expected to change with the aerosol size distribution. This again highlights the fact that we do not fully understand what is driving changes in b.

[123] 3. How do the uncertainties in the aerosol optical properties translate into uncertainties in radiative forcing? Here we assess the uncertainties in clear-sky, top-of-atmosphere direct aerosol radiative forcing (ΔF_{TOA}) that results from uncertainties in the following intensive optical properties: the hemispheric backscatter ratio, b; the single scatter albedo, ω; and the light scattering hygroscopic growth factor, f(RH). As discussed in section 4.5, the nominal measurement uncertainty in each of these parameters has been quantitatively assessed based on the performance characteristics of the TSI, Inc. nephelometer and the Radiance Research Particle Soot Absorption Photometer. However, the interplatform discrepancies presented herein indicate that these uncertainties may be underestimates for some parameters, so we will incorporate the larger bounds in our analysis of uncertainty in derived ΔF_{TOA}.

[124] Clear-sky forcing at 550 nm is calculated using the simplified model of *Haywood and Shine* [1995], which applies for optical depths $\tau \ll 2$:

$$\Delta F_{TOA} = -DS_o T_{at}^2 (1 - A_c)\omega\bar{\beta}\tau\left((1 - R_s)^2 - \frac{2R_s}{\bar{\beta}}\left(\frac{1}{\omega} - 1\right)\right),$$
(8)

where D is the fractional day length (fixed at 0.5), S$_o$ is the solar constant (1370 W/m^2), T$_{at}$ is the atmospheric transmission factor (fixed at 0.76), A$_c$ is the fractional cloud cover (set here to zero), ω is the single scatter albedo,

$\bar{\beta}$ is the upscatter fraction, τ is the aerosol optical depth, and R$_s$ is the surface reflectance. We do two sets of calculations, approximating forcing over the ocean (R$_s$ = 0.07) and over land (R$_s$ = 0.15) [*Conant et al.*, 2003]. The optical depth is fixed at τ = 1, so that $\Delta F_{TOA}/\tau$ is forcing per unit optical depth, or forcing efficiency. In Table 11 we show the uncertainty in $\Delta F_{TOA}/\tau$ in terms of the range in forcing efficiencies that result from independently varying ω and b and for allowing both to vary over their uncertainty ranges.

[125] Because ω is in good agreement across all platforms, the range of values used to calculate the uncertainty in ΔF_{TOA}, $\delta\Delta F_{TOA}$, is given by the mean plus/minus the measurement uncertainty in ω. For b, the range in the mean values from the three platforms' ''all data'' sets exceeds the instrumental uncertainty range so ΔF_{TOA} is calculated for the minimum and maximum measured mean values (Tables 10 and 11). Uncertainties were not assessed for f(RH), so the range in measured values is used to assess the range in forcing.

[126] The effect of hygroscopic growth is implicitly included in equation (8) since τ scales with f(RH). The magnitude of the uncertainty in ΔF_{TOA} will depend on the uncertainty in f(RH), which itself is a function of both the uncertainty in the hygroscopic growth functional form and the relative humidity at which it is evaluated. For climate forcing, the relative humidity of interest is the ambient RH. In the ACE-Asia study region, all platforms measured higher ambient RH when the aerosol was fine mode dominated than when it was coarse mode dominated, as is consistent with a coarse mode sourced in the desert. Because both ambient RH and hygroscopic growth were greatest for the high FMF$_{scat}$ category, the uncertainty in ambient extinction due to hygroscopicity will be largest when the aerosol is pollution-dominated and smallest when it is dust-dominated.

[127] Because the instrumental uncertainty in our f(RH) functions has not been determined, we will use the range in f(RH) values across the platforms as our uncertainty bounds and assume the gamma function given in equation (6) applies so that we can easily evaluate f(RH) for hydration from 40% to ambient RH. This is done for both coarse mode dominated aerosol (FMF$_{scat} \leq 0.45$; f(RH)$_{40-85\%}$ = 1.53−2.06; γ = 0.307−0.521; average ambient RH = 64%) and fine mode dominated aerosol (FMF$_{scat} \geq 0.80$; f(RH)$_{40-85\%}$ = 1.87−2.61; γ = 0.452−0.692; average ambient RH = 79%), as given in Table 9. For the coarse mode dominated case, hydration factors to ambient RH

range from 1.31 to 1.17. For the fine mode dominated case, hydration factors to ambient RH range from 2.07 to 1.61.

[128] The analysis discussed so far allows us to calculate the range in ΔF_{TOA} based on the uncertainty in the measured quantities. However, limitations in what we were able to measure also produce uncertainties in ΔF_{TOA}. These limitations are discussed here for completeness but they are not included in the uncertainty analysis for ΔF_{TOA}.

[129] First, the nephelometer measures hemispheric backscatter fraction, not upscatter fraction. Thus, in order to calculate ΔF_{TOA}, we must approximate $\bar{\beta}$ from b. Here we use the conversion suggested by *Sheridan and Ogren* [1999], which approximates the relationship given by the Mie model of *Wiscombe and Grams* [1976]:

$$\bar{\beta} = 0.0817 + 1.8495b - 2.9682b^2. \qquad (9)$$

This conversion is more likely to be in error for large, nonspherical dust whose phase function is not as well-constrained than for hydrated, spherical fine mode aerosol.

[130] Second, single scatter albedo is only measured at 550 nm so we can only calculate ΔF_{TOA} at this wavelength. For dust, ω is believed to increase significantly with wavelength in the visible range [cf. *Myhre and Stordal*, 2001] and - unlike other atmospheric aerosol - is expected to have a significant radiative impact at infrared (IR) wavelengths. This is because of dust's large size, its low ω in the IR, and because it is often lofted high into the atmosphere by the frontal systems that lift it off the desert surface. Also, aerosol high in the atmosphere generally has a longer lifetime and so has a larger cumulative radiative impact. Despite this limitation, knowing ω at 550 nm provides an important constraint, especially given that some modeling studies have derived or assigned low values of ω for dust at visible wavelengths (e.g., ω = 0.88 at 550 nm [*Myhre and Stordal*, 2001]; ω = 0.87–0.88 at 550 nm [*Pilinis and Li*, 1998]).

[131] Finally, in all cases, σ_{ap}, ω and b are derived at low RH only, not at ambient RH. For b, the primary effect of hydration will be an increase in size and possibly a change from nonspherical to spherical shape. In theory this should result in lower b, but as noted earlier the data here indicate an ambiguous relationship between b and the ACE-Asia aerosol size and shape. The effect of hydration on σ_{ap} and therefore also ω is completely unknown and may be significant [*Redemann et al.*, 2001]. The lack of information on f(RH) for σ_{ap} is probably more of a problem for constraining ambient-RH light extinction and ambient-RH ω for pollution than it is for dust. This is because 1) dust is not very hygroscopic (Figure 14), and 2) the primary source of dust is the desert so it is often carried in air masses with low RH, especially when it is above the boundary layer. For example, on the C-130, when FMF_{scat} < 0.3 the ambient RH for samples from <1 km altitude was 51 ± 26% and for samples from ≥1 km altitude it was 25 ± 22% and dust was preferentially measured aloft. On the other hand, pollution aerosol is quite hygroscopic and in the ACE-Asia study region it often resided in the moist boundary layer (Figure 15), so our lack of understanding of how σ_{ap} and ω change with RH is probably a more important limitation for these aerosol.

[132] Assessing how the measurement uncertainties translate into forcing uncertainties is instructive in that it indicates where the most useful improvements can be made to the in situ measurements. What we see (Table 11) is that our uncertainty in hemispheric backscatter fraction produces more than twice the uncertainty in ΔF_{TOA} (i.e., ~20–35% over the ocean) than does the uncertainty in single scatter albedo (i.e., ~10% over the ocean). Again, note that the former range is set by the field precision and the later by the nominal measurement uncertainty, since for b the nominal measurement uncertainty appears to be too low. Uncertainty in f(RH) yields uncertainties in forcing that are equal to the ω-induced uncertainty (~12%) when the aerosol is coarse mode dominated and comparable to the b-induced uncertainty (~30%) when the aerosol is fine mode dominated. These results are notable in that a great deal of attention has been paid to the in situ measurement of aerosol single scatter albedo, but there has been little discussion of how well we can constrain hemispheric backscatter fraction. Further, the range of measured values of ω was smaller than the laboratory-estimated measurement uncertainty used to bound ω in this analysis of $\delta\Delta F_{TOA}$, so ω (and therefore ΔF_{TOA}) may in fact be even more well-constrained than is indicated here. In contrast, interplatform differences in b exceed the laboratory-estimated uncertainty for reasons we do not understand. This is particularly striking in that all measurements of b were made using the same instrument. This suggests that work is needed in understanding the TSI, Inc. nephelometer measurements of hemispheric backscatter fraction and/or our theoretical understanding of how b changes with aerosol size and shape.

[133] In a similar comparison study for the INDOEX field campaign, interplatforms discrepancies in $\omega_{D<10\mu m}$ were 3% and 12%, or differences of up to 0.10 [*Clarke et al.*, 2002]. These are much larger than both the <0.02 interplatform discrepancies seen here and the ~0.025 uncertainty in ω. Note that a 10% uncertainty in ω produces a large uncertainty in ΔF_{TOA} - about 30%. In contrast, the interplatform discrepancies in b during INDOEX were smaller than those seen here: at most ~10%, or ~0.010 for b = 0.110 (typical of the INDOEX aerosol), producing an uncertainty in ΔF_{TOA} of ~15%. This was for a fine mode dominated aerosol, which is the size range of aerosol where we had the largest discrepancies in b during ACE-Asia.

9. Conclusions

[134] Results have been presented for multiple side-by-side comparisons and a campaign-wide ensemble comparison of aerosol optical properties as measured in situ from airborne (NCAR C-130 and CIRPAS Twin Otter) and surface (NOAA ship RV Ron Brown and Gosan, Jeju Island, South Korea) platforms during the ACE-Asia campaign. Because there are multiple side-by-side comparisons for pairs of these platforms we are able to distinguish between systematic biases and sporadic errors as well as state with confidence where there was good agreement. The combination of direct and ensemble comparisons further allow us to distinguish instrumental differences from real differences in the ambient aerosol sampled by the disparate platforms, each of which had a unique geographic and temporal sampling pattern. When the data are grouped so

that similar sampling regions are compared, we see that dust was more prevalent and the fine mode aerosol was more light-absorbing in the Yellow Sea than in the rest of the ACE-Asia study region.

[135] Using the campaign-wide data sets we also have given best-guess values for the Ångström exponent, single scatter albedo, hemispheric backscatter fraction, and aerosol hygroscopicity for the ACE-Asia aerosol (Table 10). The nominal measurement uncertainties, RMS error field precision, and campaign-wide interplatform ranges are used to distinguish between the accuracy of the measurements, their precision, differences due to inlet/sampling efficiency differences, and differences that arise from each platform having a unique geographic and temporal sampling regime. We also have noted that there may be differences between the in situ derived optical properties and the ambient aerosol optical properties and have attempted to constrain these differences. Finally, we have done a simple calculation to show how uncertainties in the aerosol optical properties from our in situ measurements propagate to uncertainties in top-of-atmosphere radiative forcing at 550 nm.

[136] The comparisons presented confirm that the C-130's Low Turbulence Inlet had sampling efficiencies >1.0 for coarse mode aerosol, as was expected. However, interplatform discrepancies of total aerosol light scattering generally exceeded the expected 5% enhancement for mixed aerosol. This suggests that the inlets on the some of the other platforms may have had significant losses for coarse mode, but tests of the inlet sampling efficiencies for aerosols in the $D = 2-10$ μm size range would be needed to confirm this.

[137] Interplatform differences in single scatter albedo (ω) were small. Further, ω at 550nm appears to be well constrained for both the $D < 1$ μm aerosol when it was fine mode dominated (i.e. when $\omega_{D<1\mu m}$ best approximates ω of the fine mode; $\omega_{D<1\mu m} = 0.885 \pm 0.023$) and for the $D > 1$ μm aerosol when it was fine mode dominated (i.e. when $\omega_{D>1\mu m}$ best approximates ω of the coarse mode; $\omega_{D>1\mu m} = 0.957 \pm 0.031$). Because the coarse mode aerosol was predominantly dust for most of the campaign, this implies a higher single scatter albedo for dust (0.96) than has been used in many modeling studies of dust radiative effects. On the other hand, the high single scatter albedo for dust implied in the present study is consistent with numerous previous in situ measurements. This issue has significant implications for constraining the top-of-atmosphere radiative forcing of dust, which spanned both positive and negative values in the most recent IPCC report [IPCC, 2001]. However, the wavelength-dependence of ω for dust will need to be determined before its full radiative impact can be constrained. The dependence of ω on relative humidity also needs to be determined, though this is probably a more significant factor for the ACE-Asia fine mode aerosol than for the region's dust because the latter appears not to be very hygroscopic and because it is often carried in air masses with low RH. If future studies indicate that the in situ ω measurements accurately represent the ambient aerosol, the uncertainty bounds of this parameter will be further tightened, as we have shown that it can be measured with very high precision.

[138] Interplatform discrepancies for aerosol hydration and backscatter fraction that greatly exceed the nominal measurement uncertainties indicate the need for further studies of these measurements. Further, TOA radiative forcing calculations show that the interplatform range of values for b and f(RH) (when the aerosol is fine mode dominated) produce about twice the uncertainty in ΔF_{TOA} as do the uncertainties in ω. This is notable in that the in situ measurements of ω are typically considered less robust than the in situ measurements of b and f(RH).

[139] Discrepancies in hygroscopicity were most pronounced when comparing data from a two-point system using Radiance Research nephelometers against a scanning-RH system employing TSI, Inc. nephelometers. Several possible sources of error in the ACE-Asia measurements have been considered but could not reasonably account for the observed discrepancies. Side-by-side comparisons of these two systems in a lab environment using aerosol with known hydration properties should reveal whether one or both of the systems has an inherent problem.

[140] Large interplatform discrepancies in the hemispheric backscatter fraction, b, also need to be explained. Two aspects of the data are not understood. First, interplatforms discrepancies consistently exceeded the nominal instrumental measurement uncertainties. This suggests that we do not fully understand the precision of the measurement. Second, Mie calculations predict that b decreases with increasing aerosol size, but on all three platforms where it was measured, b increased as the relative fraction of coarse mode aerosol increased. It is unclear whether this is a measurement artifact (i.e. incorrect angular truncation correction of total scatter in the nephelometer) or is due to shape effects (i.e. nonspherical coarse mode dust scattering more radiation into the backward hemisphere than would spherical aerosol).

[141] Models used to calculate direct forcing [cf. Conant et al., 2003; Haywood and Shine, 1995] and to invert satellite data typically use size distributions and a Mie model to determine the up-scatter fraction for incident light. The large uncertainties in forcing given here due to uncertainties in b could lead one to conclude that this modeling approach gives more well-constrained results than do our direct optical data. However, uncertainties in the size data and uncertainty in the appropriateness of Mie theory for dust may be causing similarly large uncertainties in the model results. Aerosol sizes are measured via their mobility (at smaller diameters) and via their aerodynamic or optically effective size (at larger diameters). When the aerosol particles are nonspherical and/or have a poorly constrained index of refraction (such as with dust and soot, both of which were present in abundance in the ACE-Asia study region) and when the mixing state is ambiguous (as it was for the ACE-Asia aerosol), it is unclear how to interpret these data quantitatively. Further, the data presented here indicate that b may increase in the presence of coarse mode dust, which is counter to what would be predicted by Mie theory. Thus Mie theory may be under-predicting the up-scatter fraction for coarse mode aerosol.

[142] Finally, we note that it is only because we had multiple comparisons available for analysis that we were able to rigorously test the in situ measurements. We strongly encourage organizers of future field experiments to make direct interplatform comparisons a priority, as the results herein will not necessarily apply directly to other aerosol types. Further, a similar comparison study of satellite-

derived optical properties from disparate satellites would allow for similarly robust conclusions about the strengths and weaknesses of their retrievals. This, combined with the results herein, would be extremely helpful in generating a unified picture of how well we, as a community, can constrain aerosol optical properties.

References

Anderson, T. L., and J. A. Ogren (1998), Determining aerosol radiative properties using the TSI 3563 integrating nephelometer, *Aerosol Sci. Technol.*, 29, 57–69.

Anderson, T. L., et al. (1996), Performance characteristics of a high-sensitivity, three-wavelength, total scatter/backscatter nephelometer, *J. Atmos. Oceanic Technol.*, 13, 967–986.

Anderson, T. L., S. J. Masonis, D. S. Covert, N. C. Ahlquist, S. G. Howell, A. D. Clarke, and C. S. McNaughton (2003), Variability of aerosol optical properties derived from in situ aircraft measurements during ACE-Asia, *J. Geophys. Res.*, 108(D23), 8647, doi:10.1029/2002JD003247.

Bates, T. S., D. J. Coffman, D. S. Covert, and P. K. Quinn (2002), Regional marine boundary layer aerosol size distributions in the Indian, Atlantic, and Pacific Oceans: A comparison of INDOEX measurements with ACE-1, ACE-2, and Aerosols99, *J. Geophys. Res.*, 107(D19), 8026, doi:10.1029/2001JD001174.

Berner, A., C. H. Lurzer, F. Pohl, O. Preining, and P. Wagner (1979), The size distribution of the urban aerosol in Vienna, *Sci. Total Environ.*, 13, 245–261.

Bond, T. C., T. L. Anderson, and D. Campbell (1999), Calibration and intercomparison of filter-based measurements of visible light absorption by aerosols, *Aerosol Sci. Technol.*, 30, 582–600.

Carrico, C. M., M. J. Rood, and J. A. Ogren (1998), Aerosol light scattering properties at Cape Grim, Tasmania, during the First Aerosol Characterization Experiment (ACE 1), *J. Geophys. Res.*, 103(D13), 16,565–16,574.

Carrico, C. M., M. J. Rood, J. A. Ogren, C. Neususs, A. Wiedensohler, and J. Heintzenberg (2000), Aerosol optical properties at Sagres, Portugal during ACE-2, *Tellus, Ser. B*, 53(2), 694–715.

Carrico, C. M., P. Kus, M. J. Rood, P. K. Quinn, and T. S. Bates (2003), Mixtures of pollution, dust, sea salt, and volcanic aerosol during ACE-Asia: Radiative properties as a function of relative humidity, *J. Geophys. Res.*, 108(D23), 8650, doi:10.1029/2003JD003405.

Clarke, A. D., and R. J. Charlson (1985), Optical properties of the background aerosol: The absorption component of extinction, *Science*.

Clarke, A. D., J. N. Porter, F. Valero, and P. Pilewski (1996), Vertical profiles, aerosol microphysics, and optical closure during ASTEX: Measured and modeled column optical properties, *J. Geophys. Res.*, 101, 4443–4453.

Clarke, A. D., V. Kapustin, W. Collins, P. Rasch, K. Moore, S. Howell, and H. Fuelberg (2001), Dust and pollution transport on global scales: Aerosol measurements and model predictions, *J. Geophys. Res.*, 106(D23), 32,555–32,569.

Clarke, A. D., et al. (2002), The INDOEX aerosol: A comparison and summary of microphysical, chemical, and optical properties observed from land, ship, and aircraft, *J. Geophys. Res.*, 107(D19), 8033, doi:10.1029/2001JD000572.

Clarke, A. D., et al. (2004), Size-distributions and mixtures of dust and black carbon aerosol in Asian outflow: Physio-chemistry and optical properties, *J. Geophys. Res.*, 109, D15S09, doi:10.1029/2003JD004378.

Conant, W. C., J. H. Seinfeld, J. Wang, G. R. Charmichael, Y. Tang, I. Uno, P. J. Flatau, K. M. Markowicz, and P. K. Quinn (2003), A model for the radiative forcing during ACE-Asia derived from CIRPAS Twin Otter and R/V Ronald H. Brown data and comparison with observations, *J. Geophys. Res.*, 108(D23), 8661, doi:10.1029/2002JD003260.

Gao, S., D. A. Hegg, D. S. Covert, and H. Jonsson (2003), Aerosol chemistry, and light-scattering and hygroscopicity budgets during outflow from East Asia, *J. Atmos. Chem.*, 46, 205.

Haywood, J. M., and K. P. Shine (1995), The effect of anthropogenic sulfate and soot aerosol on the clear sky planetary radiation budget, *Geophys. Res. Lett.*, 22, 603–606.

Haywood, J. M., P. Francis, S. Osborne, M. Glew, N. Loeb, E. Highwood, D. Tanré, G. Myhre, P. Formenti, and E. Hirst (2003), Radiative properties and direct radiative effect of Saharan dust measured by the C-130 aircraft during SHADE: 1, *Solar spectrum, J. Geophys. Res.*, 108(D18), 8577, doi:10.1029/2002JD002687.

Huebert, B. J., T. Bates, P. B. Russell, G. Shi, Y. J. Kim, K. Kawamura, G. Carmichael, and T. Nakajima (2003), An overview of ACE-Asia: Strategies for quantifying the relationship between Asian aerosols and their climatic impacts, *J. Geophys. Res.*, 108(D23), 8633, doi:10.1029/2003JD003550.

Huebert, B. J., et al. (2004), PELTI: Measuring the passing efficiency of an airborne low turbulence aerosol inlet, *Aerosol Sci. Technol.*, 38(8), 803–826.

Intergovernmental Panel on Climate Change (IPCC) (2001), Third assessment report of the Intergovernmental Panel on Climate Change, Beijing.

Jacob, D. J., J. H. Crawford, M. M. Kleb, V. E. Connors, R. J. Bendura, J. L. Raper, G. W. Sasche, J. C. Gille, L. Emmons, and C. L. Heald (2003), Transport and Chemical Evolution over the Pacific (TRACE-P) Mission: Design, execution, and first results, *J. Geophys. Res.*, 108(D20), 9000, doi:10.1029/2002JD003276.

Kalashnikova, O. V., and I. N. Sokolik (2002), Importance of shapes and compositions of wind-blown dust particles for remote sensing at solar wavelengths, *Geophys. Res. Lett.*, 29(10), 1398, doi:10.1029/2002GL014947.

Kaufman, Y. J., D. Tanré, O. Dubovik, A. Karnieli, and L. A. Remer (2001), Absorption of sunlight by dust as inferred from satellite and ground-based remote sensing, *Geophys. Res. Lett.*, 28(8), 1479–1482.

Lafleur, B. G. (1998), A low turbulence inlet for airborne aerosol sampling, M.S. thesis, Univ. of Denver, Denver, Colo.

Masonis, S. J., K. Franke, A. Ansmann, D. Müller, D. Althausen, J. Ogren, A. Jefferson, and P. Sheridan (2002), An intercomparison of aerosol light extinction and 180° backscatter as derived using in situ measurements and Raman lidar during the INDOEX field campaign, *J. Geophys. Res.*, 107(D19), 8014, doi:10.1029/2000JD000035.

Moore, K. G., II, et al. (2004), A comparison of similar aerosol measurements made on the NASA P-3B, DC-8, and NSF C-130 aircraft during TRACE-P and ACE-Asia, *J. Geophys. Res.*, 109, D15S15, doi:10.1029/2003JD003543.

Myhre, G., and F. Stordal (2001), Global sensitivity experiments of the radiative forcing due to mineral aerosols, *J. Geophys. Res.*, 106(D16), 18,193–18,204.

Pilinis, C., and X. Li (1998), Particle shape and internal inhomogeneity effects on the optical properties of tropospheric aerosols of relevance to climate forcing, *J. Geophys. Res.*, 103(D4), 3789–3800.

Quinn, P. K., et al. (2004), Aerosol optical properties measured on board the Ronald H. Brown during ACE-Asia as a function of aerosol chemical composition and source region, *J. Geophys. Res.*, 109, D19S01, doi:10.1029/2003JD004010.

Redemann, J., P. Russell, and P. Hamill (2001), Dependence of aerosol light absorption and single-scattering albedo on ambient relative humidity for sulfate aerosols with black carbon cores, *J. Geophys. Res.*, 106(D21), 27,485–27,495.

Redemann, J., S. J. Masonis, B. Schmid, T. L. Anderson, P. B. Russell, J. M. Livingston, O. Dubovik, and A. D. Clarke (2003), Clear-column closure studies of aerosol and water vapor aboard the NCAR C-130 in ACE-Asia, 2001, *J. Geophys. Res.*, 108(D23), 8655, doi:10.1029/2003JD003442.

Schmid, B., et al. (2003), Column closure studies of lower tropospheric aerosol and water vapor during ACE-Asia using airborne Sun photometer

and airborne in situ and ship-based lidar measurements, *J. Geophys. Res.*, *108*(D23), 8656, doi:10.1029/2002JD003361.

Sheridan, P. J., and J. A. Ogren (1999), Observations of the vertical and regional variability of aerosol optical properties over central and eastern North America, *J. Geophys. Res.*, *104*, 16,793–16,805.

Sheridan, P. J., D. J. Delene, and J. A. Ogren (2001), Four years of continuous surface aerosol measurements from the Department of Energy's Atmospheric Radiation Measurement Program Southern Great Plains Cloud and Radiation test bed site, *J. Geophys. Res.*, *106*, 20,735–20,747.

Wang, J., et al. (2002), Clear-column radiative closure during ACE-Asia: Comparison of multiwavelength extinction derived from particle size and composition with results from Sun photometry, *J. Geophys. Res.*, *107*(D23), 4688, doi:10.1029/2002JD002465.

Wiscombe, W. J., and G. W. Grams (1976), The backscattered fraction in two-stream approximations, *J. Atmos. Sci.*, *33*, 2440–2451.

———————————

T. L. Anderson, S. J. Doherty, and D. Hegg, Department of Atmospheric Science, University of Washington, Box 351640, Seattle, WA 98195, USA. (sarahd@atmos.washington.edu)

C. M. Carrico, Department of Atmospheric Science, Colorado State University, Fort Collins, CO 80523-1371, USA.

A. Jefferson, NOAA-CMDL, 325 Broadway R/CMDL, Boulder, CO 80305, USA.

P. K. Quinn, NOAA-PMEL, 7600 Sand Point Way NE, Seattle, WA 98115, USA.